UNIVERSITY OF SALERNO
Department of Pharmacy

PhD program in
Drug discovery and development
XXIX Cycle — 2016/2017

PhD thesis

In vitro and in vivo study of cannabinoids as modulators of Wnt/β-catenin pathway in human colorectal cancer

PhD student   Tutor

Dr. *Donatella Fiore*   Prof. *Patrizia Gazzerro*

Coordinator: Prof. *Gianluca Sbardella*

Chapter IV. *Discussion*

References

Abstract

Colorectal cancer (CRC) is the second most common cause of cancer death. Molecular events in CRC has been extensively studied and several data suggest that Wnt/β-catenin signaling deregulation play a pivotal role in colorectal carcinogenesis. Majority of both familial syndromes (FAP) and sporadic colon cancers, arise from APC or β-catenin genes alterations, leading to Wnt signaling hyperactivation. According to the cancer stem cells (CSCs) theory, some cancer-initiating cells, harboring stem-cell like properties, evade standard chemotherapies, resulting in recurrent and metastatic tumors. Wnt/β-catenin signaling and its deregulation is involved in the recurrence and maintenance of CSCs. In recent years, understanding of molecular mechanisms underlying CSCs biology, led to development of novel strategies to completely eradicate colorectal cancer.

Some evidences suggest a potential crosstalk between the endocannabinoid system and the Wnt pathway, also in cancer stem cells, in several tumor types. This could represent a key mechanism in the control of the anti-cancer activity of cannabinoids, as well as a novel putative site for pharmacological intervention.

Results from this work led to identification of Rimonabant, originally an inverse agonist of CB1 cannabinoids receptor, as modulator of Wnt/β-catenin pathway in CRC, able to control colon cancer stemness, without toxicity toward cells from healty tissue. Moreover, for the first time, we proposed a novel epigenetic mechanism Rimonabant-mediated.

CHAPTER I

INTRODUCTION

Colorectal cancer (CRC) development is typically associated with a stepwise accumulation of specific genetic alterations, collectively known as "adenoma-carcinoma sequence". This multistep process drives the onset of pathologic alterations, ranging from microscopic lesions, such as Aberrant Crypt Foci (ACF), to metastatic phenotypes. However, in the last decades, better understanding of cancer genetic features, needed to improve colon cancer management, highlighted that adenoma-carcinoma sequence arises in a limited portion of CRC cases (about 50-60%). To date, seems to be clear that an higher genetic complexity exists, which results in elevated heterogeneity, both at inter- and intra-tumoral level (Fearon, 2011; Punt et al, 2016).

It was widely accepted that the majority of both familial syndromes (Familial Adenomatous Polyposis, FAP) and sporadic colon cancers, arise from inactivation of APC (Adenomatous Polyposis Coli) tumor suppressor gene that negatively regulates Wnt/β-Catenin pathway. APC truncation results in loss of β-Catenin-binding domain, thereby into failure of β-Catenin degradation. With high frequency, CRC with wild type APC, harbor gain of function mutation in β-Catenin gene, typically associated with loss of phosphorylation sites, required for its proteasomal degradation. This alteration seems to be related to high malignant CRC. Substantially, both APC and β-Catenin genes mutations, allow to hyperactivation of Wnt signaling (Deitrick & Pruitt, 2016; Fearon, 2011; Jhonson et al, 2005; Morin et al, 1997).

5

Wnt/β-Catenin pathway is an highly conserved signaling, known to exerts a key role not only in embryonic development and normal tissue homeostasis, but also in the most part of cancer-related processes, such as proliferation, differentiation, apoptosis, and cell survival (Anastas & Moon, 2013). Tissue- and contest-specific, Wnt pathway consists of ligands and receptors that orchestrate an intricate signal transduction. Wnt ligands family includes about 19 members for about 10 Frizzled receptors. The signaling across plasma membrane can be transduced through canonical pathway (β-Catenin-dependent) and non-canonical pathway (β-Catenin-independent). In canonical signaling, the absence of Wnt ligands culminates with constitutive β-Catenin degradation. A multiprotein cytoplasmic complex consisting of casein kinase 1α (CK1α), Axin, glycogen synthase kinase 3 (GSK3) and APC, promotes β-Catenin phosphorylation, tag for its ubiquitination and proteasomal degradation. Canonical ligands, such as Wnt3, bind Frizzled (Fzd) receptor and low density Lipo protein Receptor-related Protein 5 (LRP5) or LRP6 co-receptor to phosphorylate Dishvelled (Dvl3) protein. This latter, sequestering GSK3 and Axin, leads to disruption of degradation complex, thereby blocking the degradation of β-Catenin. Once accumulated in cytoplasm, β-Catenin translocates in the nucleus where displaces Groucho transcriptional repressor and binds Lymphoid Enhancer-binding Factor (LEF) and T Cell Factor (TCF) proteins (Deitrick & Pruitt, 2016; Anastas & Moon, 2013). This culminates with transcriptional activation of downstream target genes. Some of Wnt-regulated genes, such as COX-2, c-Myc, Cyclin D1, CD44 and Lgr5 are critically involved in colorectal carcinogenesis (Herbst et al, 2014).

Non-canonical β-Catenin-independent signaling, can be transduced through two mainly ways: Planar Cell Polarity (PCP) pathway and Wnt/Ca^{2+} pathway, mediated by protein kinase C (PKC) and calcium/calmodulin-dependent protein kinase II (CaMKII) (Anastas & Moon, 2013). Of note, it was reported that activation of non-canonical axis Wnt5a/Ror2/JNK, antagonize canonical

Wnt3-induced pathway. Moreover, with high frequency, Wnt5 promoter results methylated in human CRC cell lines and in human primary tumors, suggesting its potential as epigenetic biomarker or therapeutic target for CRC (Mikels & Nusse, 2006; Ying et al, 2008).

In addition to TCF/LEF transcription factor, β-Catenin nuclear activity downstream canonical signaling, includes binding with several other proteins. The complex transcriptional machinery regulated by β-Catenin on Wnt Responsive Elements (WRE), includes among others p300 (Kat3b) and CREB-binding protein (CBP or Kat3a) co-activators. p300 and CBP are two high-related proteins, able to coordinate chromatin remodeling complex through their histone lysine acetyltransferases (HAT) catalytic activity (Mosimann et al, 2009). Despite their high homology, CBP and p300 seem to play a non-redundant role in cell proliferation and differentiation, but several reports demonstrated that both CBP-selective (ICG-001 and PRI-724) and CBP/p300 non-selective (C646) inhibitors are able to exert their antitumor effects in CRC, counteracting β-Catenin binding and transcriptional activity on WRE (Bordonaro & Lazarova, 2016; Gaddis et al, 2015).

Although alterations in Wnt/β-Catenin signaling players were found in the most of CRC, it is now clear that only Cancer Stem Cells (CSCs), Wnt hyperactive subset of cells within tumor bulk, retain tumorigenic ability, supporting hierarchical organization of CRC. Self-renewal, loss of differentiation, high resistance to a large part of chemotherapeutics and iper-expression of specific markers (such as c-Myc, CD133, CD44, Lgr5) are typical features of CSCs. It's widely accepted that in high malignancy, chemoresistance and thus relapses onset are certainly ascribable to cancer stem cells (Zeuner et al, 2014; Todaro et al, 2010; Vermeulen et al, 2010; O'Brien et al, 2007). In recent years, understanding of molecular mechanisms underlying CSCs biology, led to development of novel strategies to completely eradicate colorectal cancer, also for high malignant CRC.

To date, several compounds able to target Wnt pathway in CRC and other tumors, have been identified, including cannabinoids. DeMorrow and colleagues, in 2008 reported that anandamide (AEA), a cannabinoid receptor 1 (CB1) agonist, inhibits cholangiocarcinoma growth through activation of the non-canonical Wnt pathway. In addition, a stable analogue of endogenous anandamide (Met-F-AEA) inhibits β-Catenin transcriptional activity in human breast cancer cells, repressing TCF/LEF promoter activation (Laezza et al, 2010). More interesting, some reports demonstrated the ability of cannabinoids to inhibit gliomagenesis targeting glioma stem cells (GSCs) (Aguado et al, 2007; Nabissi et al, 2015) and inhibit spheroid formation in prostate cancer stem cells (Sharma et al, 2014).

Antitumor action of cannabinoids in CRC, was strongly supported by several authors. The Endocannabinoid (EC) system role in the progression of colorectal cancer has been analyzed *in vivo* (Izzo AA et al., 2008; Santoro et al, 2009) were cannabinoids-mediated reduction of precancerous lesions in the mouse colon was found. In CRC cells, with different mechanisms, both CB1 and CB2 agonist, as well as antagonists showed antitumor action, inducing cell death mechanisms ranging from apoptosis to mitotic catastrophe (Greenhough et al, 2007; Cianchi F et al, 2008; Izzo AA et al, 2008; Santoro et al, 2009). Intriguingly, Proto and colleagues, in 2012, demonstrated that in colon cancer cells cannabinoids modulate CB1 and estrogen receptors (ERs), whose loss might promote and accelerate colorectal carcinogenesis in APCMin/+ mice (Proto et al, 2012; Wang et al, 2008). Finally, cannabinoids improve the efficacy of chemotherapic drugs used in the clinical practice (Gustafsson et al, 2009; Gazzerro et al, 2010).

Here, for the first time, we investigated *in vitro* and *in vivo* the hypothesis that the antitumor effects of cannabinoids in CRC could be due to direct modulation of Wnt/β-Catenin pathway. Moreover, cannabinoids effects on primary colon cancer stem cells and chemoresistance have been examined.

CHAPTER II

MATERIALS AND METHODS

2.1   General materials.

Rimonabant (also referred as SR141716 or SR) was kindly donated by Sanofi-Aventis (Montpellier, France). It was dissolved in DMSO and added to cells cultures at the indicated concentrations. 2-Methyl-2'-Fluoro Anandamide (Met-F-AEA), 5-Fluorouracil and Oxaliplatin were purchased from Sigma-Aldrich (Dorset, UK). CB13 and CB74 were synthetized and kindly donated by Prof. Clementina Manera (Dept. of Pharmacy, University of Pisa) (fig. 1).
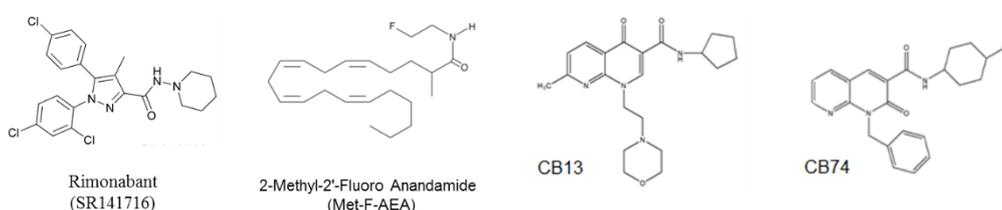
Figure 1. Chemical structures of cannabinoid compounds.

Anti-caspase-3 and cleaved caspase 3, anti-PARP [poly (ADP-ribose) polymerase], anti-GAPDH, anti-phospho-β-Catenin, anti-Wnt3, anti-LRP6, anti-phospho-GSK3β (Ser9), anti-GSK3β, anti-CaMKII, anti-c-Myc and anti-COX-2 antibodies were all from Cell Signaling Technology (Danvers, MA, USA); anti-β-Catenin, anti-Dvl3, anti-Fzd7, anti-APC, anti-Wnt5A, anti-ROR2, anti-phospho-CaMKII, anti-Lgr5, anti-acetyl histone H3 and anti-acetyl histone H4 were from Abcam (Cambridge, UK). Anti-Cyclin D1 and

anti-Lamin A/C were purchased and Sigma-Aldrich (Dorset, UK), respectively. Secondary HRP-linked goat anti-mouse or goat anti-rabbit IgG, were also purchased from Cell Signaling Technology (Danvers, MA, USA). Anti-Annexin V-FITC, anti-CD133-PE, anti-CD44-FITC were from Miltenyi biotec.

2.2 Cell cultures, treatments and viability assay.

Human CRC cells DLD1, SW620, SW48 and HCT116 were obtained from the Interlab Cell Line Collection (IST, Genoa, Italy). DLD1 cells were routinely grown in RPMI-1640, SW620 cells in Dulbecco's modified Eagle medium (DMEM), SW48 in DMEM-F12 and HCT116 cells in McCoy's 5A medium, supplemented with 10% fetal bovine serum (FBS), 1% non-essential amino acids, 2 mM glutamine, 100 U/ml penicillin, 100 µg/ml streptomycin, in monolayer culture and incubated at 37˚C in a humidified atmosphere containing 5% CO_2. Cells were exposed to various concentrations of compounds for the times showed in the figures and to evaluate cells viability the colorimetric MTT metabolic activity assay was used. To this aim, MTT stock solution (5 mg/ml in PBS, Sigma) was added to each well and incubated for 4 h at 37˚C in humidified CO_2. At the end of the incubation, the medium was removed and the formazan crystals were solubilized with acidic isopropanol (0.1 N HCl in absolute isopropanol). MTT conversion to formazan by metabolically viable cells was monitored by spectrophotometer at an optical density of 570 nm. Each data point represents the average of three separate experiments in triplicate.

2.3 Cell cycle and FACS analysis.

To assess cell cycle profiles, HCT116 cells ($2,5x10^4$/6cm plate) were treated for 24 and 48h with Rimonabant 10µM or vehicle alone. At the end of treatments they were collected, fixed in 70% ethanol and kept at -20 °C

overnight. Propidium iodide (PI; 50 μg/ml) in ice-cold phosphate-buffered saline (PBS) was added to the cells for 15 min at room temperature. The cells were acquired by a FACS-Calibur flow cytometer (BD Biosciences). Analysis was performed with ModFit LT v3.2 (Verity Software House).

For FACS analysis of apoptosis induction, HCT116 cells were double stained with FITC-conjugated Annexin V (BioLegend) in a binding buffer (10 mM HEPES/NaOH, pH 7; 140 mM NaCl; 2.5 mM CaCl2) for 20 min at room temperature and then with PI for additional 15 min in the dark. The cells were analyzed on a FACS-Calibur flow cytometer (BDIS, Becton Dickinson). FITC and propidium iodide emissions were detected in the FL-1 and FL-2 channels, respectively. For each sample, at least 20000 cells were recorded and subsequent analysis was performed with FlowJo® software (BDIS).

2.4 Western blot analysis.

Total protein extracts were obtained through lysis in buffer A (50 mM Tris–HCl pH8.0 buffer containing 150 mM NaCl, 1% Nonidet P-40, 2 mg/ml aprotinin, 1 mg/ml pepstatin, 2 mg/ml leupeptin, 1 mM Na_3VO_4). Protein concentration was determined by the Bradford assay using bovine serum albumin as standard. 10-30 μg of proteins were loaded were subjected to 8-12 % SDS-PAGE, under reducing conditions. Gels were electroblotted into nitrocellulose membranes (Millipore Co) and filters were probed with the primary antibodies indicated in general materials.

Subcellular fractionation of cytoplasmic and nuclear protein extracts was obtained by using NE-PER® Nuclear and Cytoplasmic Extraction Reagents (Thermo scientific). Immunoreactive bands were quantified with Image Lab analysis software (Bio-Rad).

2.5   Luciferase assay.

HCT116 cells were transiently cotransfected with an inducible transcription factor-responsive construct encodes the *Firefly* luciferase reporter gene under the control of a basal promoter element (TATA box) containing tandem repeats of TCF/LEF Response Element (TRE). To normalize transcription efficiency a constitutively expressing *Renilla* construct encoding the *Renilla* luciferase reporter gene under the control of a CMV immediate early enhancer/promoter was used. As negative control we used non-inducible reporter construct encodes firefly luciferase under the control of a basal promoter element (TATA box), without any additional transcriptional response elements. Finally, to evaluate transcription efficiency, constitutively expressing GFP construct was used. All constructs were purchased from Quiagen and used according to manufacturer's protocol. Mixture of above described constructs was distributed as shown in figure 2. Transcription
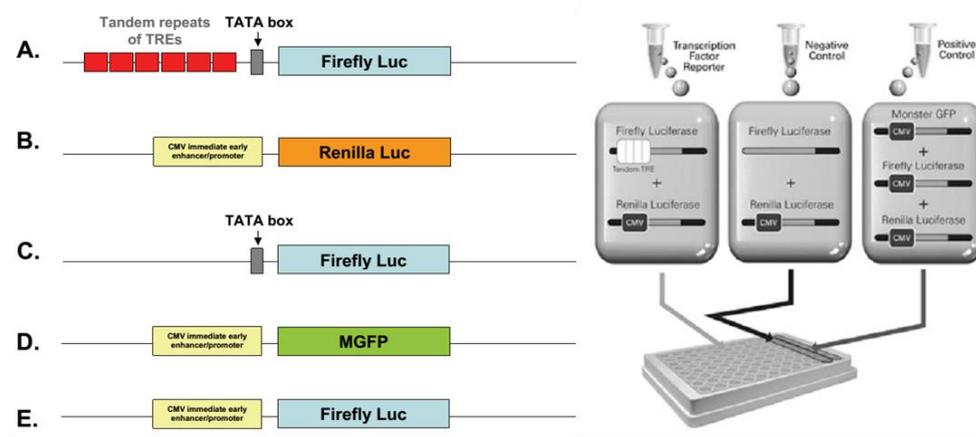
Figure 2. Schematic representation of constructs and their distribution (from Quiagen.com)

efficiency was calculated as percentage of GFP expressing cells versus total cells (mean of cellular counts performed in at least 5 microphotographs from 4 independent experiments). Luciferase activity was measured using a dual luciferase assay system (Promega), according to manufacturer's instruction

and read with an EnSpire-2300 luminometer (Perkin Elmer). Relative firefly luciferase activity was obtained by normalizing it to that of *Renilla* luciferase activity.

2.6   Confocal microscopy.

Cells were grown on slides in 12 well plates (3 x 104 cells/well). After treatment, cells were fixed in parafolmadehyde (PFA, 3,7% v/v in PBS) for 15 minutes, washed and permeabilized in Tryton X-100 (0,1% v/v in PBS) for 10 minutes. Then, cells were blocked with 4% Bovine Serum Albumin (BSA) for 1 h at room temperature and incubated with anti-β-Catenin (ab32572 Abcam; 1:250) and Anti Lamin A/C (SAB4200236 Sigma-Aldrich; 1:250) primary antibody, at 4° C overnight. Immunofluorescence staining was obtained by incubating for 90 minutes with Alexa Fluor® 488 donkey anti-rabbit IgG (A21206, Molecular Probes®; 2 µg/ml) and Alexa Fluor® 594 goat anti-mouse IgG (A11032, Molecular Probes®; 1 µg/ml) secondary antibodies. The slides were mounted using mowiol mounting medium; a Zeiss LSM 510 Laser Scanning Microscope (Carl Zeiss MicroImaging GmbH, Jena, Germany) for data acquisition was used. Samples were vertically scanned from the bottom of the coverslip with a total depth of 5 μm and a Plan-Apochromat oil-immersion objective (magnification 63X*1.7; 1.40 NA). A total of 10 z-line scans with a step distance of 0.5 μm were collected and single planes or maximum-intensity z-projection of stacks and an orthogonal projection (=xy, xz, yz planes for z-stacks series) were generated with Zeiss LSM Image Examiner Confocal Software (Carl Zeiss MicroImaging GmbH).

2.7   Semiquantitative RT-PCR.

Total RNA extraction, cDNA synthesis and reverse-transcription PCR were performed as described in Proto et al, 2012. The specific primer pairs used for

β-Catenin gene were: F 5'-GTCCGCATGGAAGAAATAGTTGA-3', R 5'-AGCTGGTCAGCTCAACTGAAAG-3'

All reactions were performed at least in triplicate; the PCR products were quantified with Image Lab analysis software (Bio-Rad) and results were normalized to those obtained from ActinB.

2.8 Drug combination analysis.

The relative contribution of Rimonabant and 5-FU to the anti-proliferative effect in HCT116 cells and establishment of pharmacological interaction type, were calculated using Compusyn, dedicated software based on Chou-Talalay method (Chou & Talalay, 1984). Through median-effect equation, that is the common-link for single and multiple ligand interactions, this software allow calculation of Combination Index (CI) to define synergism (CI<1), additive effect (CI=1) and antagonism (CI>1). Moreover, Dose reduction index (DRI) representing the measure of how much the dose of each drug in a combination may be reduced at a given effect level compared with the doses of each drug alone (Chou, 2010). Assessment of drug interactions was performed calculating CI after treatment for 24h with 1:2.5 Rimonabant/5-FU in combination and as single drugs. The treatments were performed at least in triplicate, in three independent experiments.

2.9 Inverse Virtual Screening.

The chemical structures of investigated compounds (SR141716, plus 30 "blank" compounds) were built with Maestro (version 10.2, Schrödinger, LLC, New York, NY, 2015) Build Panel. Prior to perform molecular docking calculations, optimizations (Conjugate Gradient, 0.05 Å convergence threshold) of the structures were applied to identify possible three-dimensional models. Then, all the structures were converted in the .pdbqt format using

OpenBabel software (version 2.3.2) (O'Boyle et al, 2011), adding Gasteiger charges.

306 protein 3D structures were prepared downloading the .pdb files from the Protein Data Bank database (www.rcsb.org). For each structure, "non-structural" water molecules were removed, and the processed file was then converted in .pdbqt format, merging non polar hydrogens and adding Gasteiger charges.

Molecular docking calculations were performed using the Autodock-Vina software (Trott & Olson, 2010). In the configuration files linked to 3D structures of the protein, coordinates and dimensions along x,y,z axes of the grid related to the site of presumable pharmacological interest, with spacing of 1.0 Å between the grid points. The exhaustiveness value was set to 64, saving 10 conformations as maximum number of binding modes. For all the investigated compounds, all open-chain bonds were treated as active torsional bonds.

A first set of promising interacting proteins of SR141716 was selected setting a predicted binding affinity cutoff = -7.5 kcal/mol. The identified proteins (166 items) were then also screened against "blank" molecules, the latter needed for the normalization (Lauro et al, 2012; Lauro et al, 2011) of the binding affinities of SR141716, as reported in equation 1:

$$V = V_0/V_R \text{ [eq. 1]}$$

where, for each target investigated, V represents the normalized value of SR141716, V_0 is its predicted binding affinity from docking calculations (kcal/mol), V_R is the average value of binding energy calculated on all the "blanks" (kcal/mol). It is important to note that V is a dimensionless number, and then it can be used to predict the interacting targets of a case-study compound, rather than to have precise indications about the related binding

affinities. After the normalization process, a final ranking was obtained from the most to the less promising target. Normalized values and predicted binding energies for SR141716 are collected in Table S2 (Supporting Information), respectively. The ligand/protein complexes were visually inspected with Maestro (version 10.2). Illustrations of the 3D models were generated using Maestro (version 10.2).

2.10   Kat3B/p300 activity assay.

To evaluate Rimonabant effects on intrinsic acetyltransferase activity of p300, fluorimetric cell-free assay was performed with recombinant p300 in the presence of SR141716, AVE1625 (Drinabant, another selective CB1 receptor inhibitor), anacardic acid (used as inhibitor control) or vehicle alone. Histone H3 peptide and Acetyl CoA were used as acetylation substrates and the fluorescence amplified by a thiol detecting probe was measured at Ex/Em = 392/482 nm with an EnSpire 2300 multimode plate reader. Measurements were performed in triplicate for each treatment, and the experiment was repeated at least three independent times.

Histone extracts from HCT116, DLD1 and SW48 cell lines treated with SR141716 (10μM) or with the vehicle alone were quantified for histone H3 and histone H4 global acetylation with a colorimetric assay. Global acetylation status of histones H3 and H4 were also detected through western blot analysis of total protein extracts.

2.11   *In vivo* studies.

Animals. 20 female SCID mice (SHO, 6-8 weeks old) were obtained from Charles River, maintained under clean room conditions in sterile filter top cages with Alpha-Dri bedding and housed on high-efficiency particulate air (HEPA)-filtered ventilated racks. Animals received sterile rodent chow and water *ad libitum*. All experimental procedures were conducted in accordance

with the Institute for Laboratory Animal Research Guide for the Care and Use of Laboratory Animals. The experimental protocols received the approval of the Ethical Committee of the Italian Board of Health (prot. n. 0031993 and n. 0031994, June, 6, 2013).

Subcutaneous xenograft models in athymic mice. HCT116 cells (1×10^6, suspended in 150 μl of PBS) were implanted subcutaneously into the right flank region of each mouse and allowed to grow to the size of approximately 50-70 mm^3. SR141716 (0,07 mg/kg/dose in 150 μl of PBS/20% Glycerol) was administered three time a week by peri-tumoral injection for 6 weeks. Animals in the corresponding control group received PBS/20% Glycerol (150 μl) peri-tumoral injected on the same schedule as SR141716. Mice were daily monitored for clinical signs and mortality. Body weight recordings were carried out bi- or three-weekly. Progress of tumors was determined by two dimensional caliper measurements, and tumor volumes were calculated using a standard hemi ellipsoid formula: [length (mm) x width (mm)^2]/2. Tumor volumes were analyzed using one-way ANOVA. At the end of the study, mice were humanely euthanized and tumors were resected and frozen immediately or fixed in 10% formalin for further analysis.

For western blot analysis, frozen tumor pieces were disrupted for protein extraction by gentle homogenization (Potter-Elvehjem Pestle) in cold RIPA buffer. About 30 μg of proteins was loaded on 12% SDS–polyacrylamide gels under reducing conditions and used for western blot analysis. For immunofluorescence staining and confocal analysis, fixed tumor pieces were OCT-embedded, sectioned (10 μm), stained with primary and secondary antibodies (diluted in PBS/1% BSA/0,05% Triton-X-100) and analyzed using a Zeiss LSM 510 Laser Scanning Microscope (Carl Zeiss MicroImaging).

2.12 GTG7 cultures.

Primary Colorectal Cancer Stem Cell line, GTG7, was kindly provided by Prof. Jan Paul Medema (Academisch Medisch Centrum (AMC), Center for Experimental and Molecular Medicine (CEMM), Laboratory of Experimental Oncology and Radiobiology (LEXOR), University of Amsterdam), obtained from patients as described in Prasetyanti et al (2013). GTG7 cells were cultured and propagated as spheroids in ultra-low adherent supports, in CSC medium (Advanced DMEM-F12) supplemented with: N2 supplement (Gibco), 6mg/ml glucose, 5mM HEPES, 2mM L-glutamine, 4µg/ml heparin, 50ng/ml Epidermal Growth Factor (EGF) and 10ng/ml basic Fibroblast Growth Factor (bFGF). GTG7 spheroids, are established cells containing a TCF/LEF-driven GFP reporter for Wnt-signaling activity (Wnt-TOP-GFP), as described in Vermeulen et al (2010). In this system, the 10% highest expressing Wnt-GFP (TOP-GFP^{high} or Wnt^{high}) represent CSCs, while the 10% lowest (TOP-GFP^{low} or Wnt^{low}) identificate differentiated tumor cells.

2.13 FACS-based Caspase 3 assay and Nicoletti assay.

To measure cell death at single cell level in Wnt^{high} (CSCs) and at the same moment, in the same experiment, in Wnt^{low} (differentiated colon cancer cells), cytofluorimetric analysis of caspase 3 activation was performed. GTG7 spheroids were dissociated as single cells and seeded in triplicate, in 12 multiwell plate (50000 cells/well) in adherent condition. After overnight adherence, cells were exposed to Rimonabant for 24 hours, at 5, 10, 15, 20 µM concentrations. At the end of treatments, GTG7 were collected as single cells using Trypsin-EDTA and washed with CSC medium. Caspase 3 activity was measured using CaspGlow active staining kit (Red-DEVD-FMK), according to manufacturer's instructions (BioVision). Briefly, after collection and washing, cells were pelleted and stained with RED-DEVD-FMK substrate for 1h at 37°C. Subsequently, cells were washed twice with wash buffer and flow

cytometry was performed with FACS Canto (BD bioscience). Cell death was measured analysing PE intensity in 10% gated Wnt-GFP[high] and 10% Wnt-GFP^{low} cells.

To measure DNA fragmentation status, Nicoletty assay was performed. Cells were seeded and collected as described above, then resuspended in Nicoletti buffer (0.1% sodium citrate (w/v) and 0.1% Triton X-100 (v/v) in deionized water pH 7.4, supplemented with 50 μg/ml propidium iodide before use). After incubation at 4°C, PI staining of nuclei was measured using flow cytometry (FACS Canto).

Measurements were performed in triplicate for each treatment, and the experiment was repeated at least three independent times. Data were analysed with FlowJo® software (BDIS)

2.14 Cell survival assay in GTG7.

Spheroids cultures of CSCs were dissociated and seeded as single cells in 12 multiwell plate (50000 cells/well). After overnight adherence, GTG7 were treated with Rimonabant as in cell death assay. At the end of treatments, they were collected after exposure with trypsin-EDTA and pelleted. For each treatment points, 20000 cells were distributed in triplicate in 96 ultalow adherent multiwell (Corning). Clones development, and then cell survival of CSCs, was measured at different time points, starting from day 0 (corresponding to 24h treatments) until day 13, through colorimetric viability assay, by adding 20 μl/well of Cell Titer Blue (CTB) reagent (Promega). After 4h of incubation, viability was monitored by spectrophotometer ($560_{Ex}/590_{Em}$ nm). Each data point represents the average of three separate experiments in triplicate. Statistical analysis was performed with GraphPad Prism software[©].

2.15   Normal colon human organoids cultures and clonogenic assay.

Normal colon human organoids culture was kindly provided by Prof. Jan Paul Medema (AMC, University of Amsterdam), obtained as described in Sato et al (2011). The crypts were cultured in matrigel, in Normal colon culture medium: advanced DMEM/F12, supplemented with N2 and B27 supplement, Pen/Strep, gentamycin, amphotericin B, 2mM GlutaMax-1, 10mM HEPES, 1mM N-acety-L-cysteine (Sigma), 10 nM [Leu15]-gastrin I (Sigma), 10mM nicotinamide (Sigma), 500nM A83-01 (Tocris), 3μM SB202190 (Sigma), 50% WNT3A conditioned medium, 50 ng/ml h-EGF, 20% RSPO1 conditioned medium, 10% Noggin conditioned medium, 10 nM PGE2 (Santa Cruz Biotechnology).

For DNA fragmentation analysis, matrigel was mechanically destroyed and crypts were resuspended in Cell Recovery solution (BD bioscience). After incubation on ice, Nicoletti assay was performed as previously described in section 13.

To assess Rimonabant effects on normal colon organoids clonogenicity, 50-100 crypts were diluted in matrigel and seeded in 24 multiwell plate. After overnight incubation in normal colon medium, organoids were counted under microscope and then treated for 24h with Rimonabant 10, 15 and 20 μM. After treatments, matrigel was mechanically destroyed, organoids were collected and pelleted to remove Rimonabant. Then, for each replicate all organoids were diluted in new matrigel and seeded again in 12 multiwell plate, with fresh medium. After 7 days, vital crypts were counted under microscope. Each data point represents the average of two separate experiments in duplicate.

2.16   Statistical analysis.

Data obtained from multiple experiments were calculated as means ± SD and analyzed for statistical significance by using the 2-tailed Student t-test, 1- or 2-way ANOVA for independent groups, with the Tukey or Bonferroni

correction for multiple comparisons. Values of P < 0.05 were considered statistically significant.

CHAPTER III

RESULTS

3.1 Cannabinoids-mediated control of human colorectal cancer cells *in vitro*.

The ability to affect cell viability was initially screened for four cannabinoids compounds in human CRC cell line HCT116. In particular, CB13 and CB74, two synthetic CB2 receptor agonists, showed any activity on cell viability, at any of used concentrations. The synthetic analogue of endogen Anandamide, 2-Methyl-2'-Fluoro Anandamide (Met-F-AEA), CB1 receptor agonist, was able to reduce significantly HCT116 cell viability after 48h treatments, starting from 10 μM (fig. 3). The most promising results were obtained with CB1 antagonist/inverse agoinist Rimonabant (SR141716). A previous work from Santoro et al (2009) showed that in DLD1 and SW620 CRC cell lines (β-Catenin wild type, APC mutant cells), Rimonabant is able to induce G2/M and S-G2/M arrest, respectively, without induction of apoptosis. In HCT116 cells (β-Catenin mutant cells) Rimonabant was able to inhibit cell growth significantly, starting from 24h treatments with 20 μM and from 5 μM after 48h treatments. Moreover, in HCT116 cells, a significant increase of Sub-G0/G1 cell phase, persistent until 48 hours, was observed after treatments with Rimonabant 10 μM (figure 4a). Cytofluorimetric analisys of PI/Annexin V-FITC double stained HCT116 cells, showed that Rimonabant induces an increase of double stained subpopulation (fig. 4b), suggesting a probable induction of apoptotic cell death. To confirm this hypothesis, western blot analysis of activated PARP and Caspase-3 was performed. Figure 4c shows
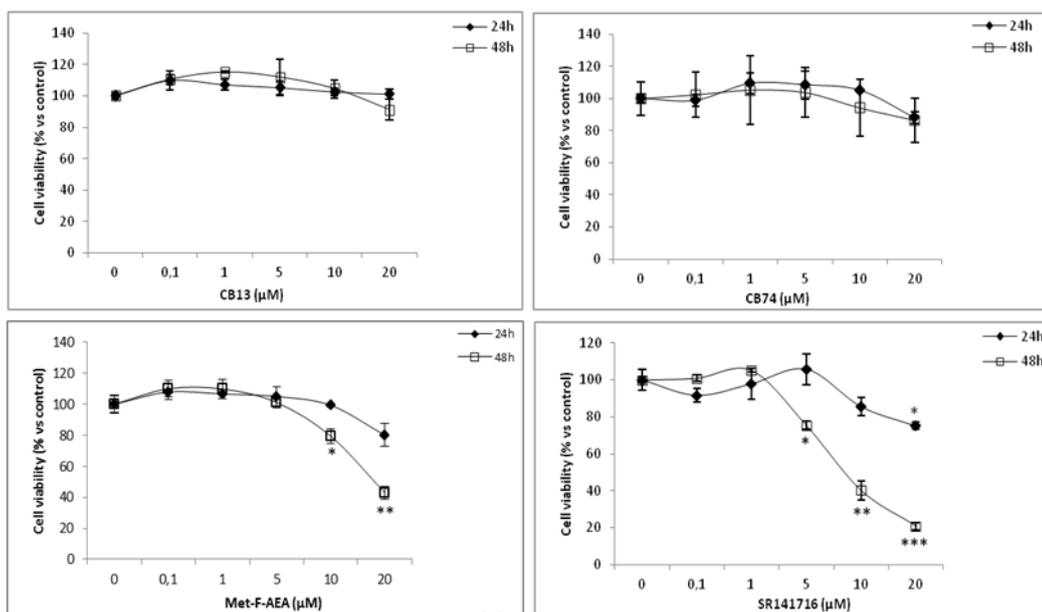
Figure 3. MTT assay in HCT116 cells treated with indicated doses of CB13, CB74, Met-F-AEA and Rimonabant (SR141716). All experiments were performed in triplicate in at least three times. The results are shown as the mean ± SD (*p<0.05, **p<0.01 and ***p<0.005).

that Rimonabant induces PARP and Caspase-3 cleavage, starting from 24 h treatments whit 10 µM. To elucidate the precise cell death mechanism induced by Rimonabant, analysis of membranes from human apoptosis antibody array was performed. Obtained results, confirmed the data obtained with western blot and showed an upregulation of Cytochrome C and of several death receptors (TRAILR-1, -2 and -3). Finally, Rimonabant was able to downregulate antiapoptotic protein Bcl-2 and X-linked Inhibitor of Apoptosis Protein (XIAP) (figure 4c).

To corroborate the results obtained in HCT116, another human CRC cell line was used. SW48 cells displays genetic profile similar to HCT116, arboring β-Catenin gene mutation and wild type APC and p53 genes. Similar to HCT116, MTT assay showed that Rimonabant significantly inhibits SW48 cells growth, after 24h at 20 µM and starting from 10 µM after 48h of treatments. Furthermore, also in the line SW48 Rimonabant was able to activate PARP and Caspase 3 (fig. 4d).
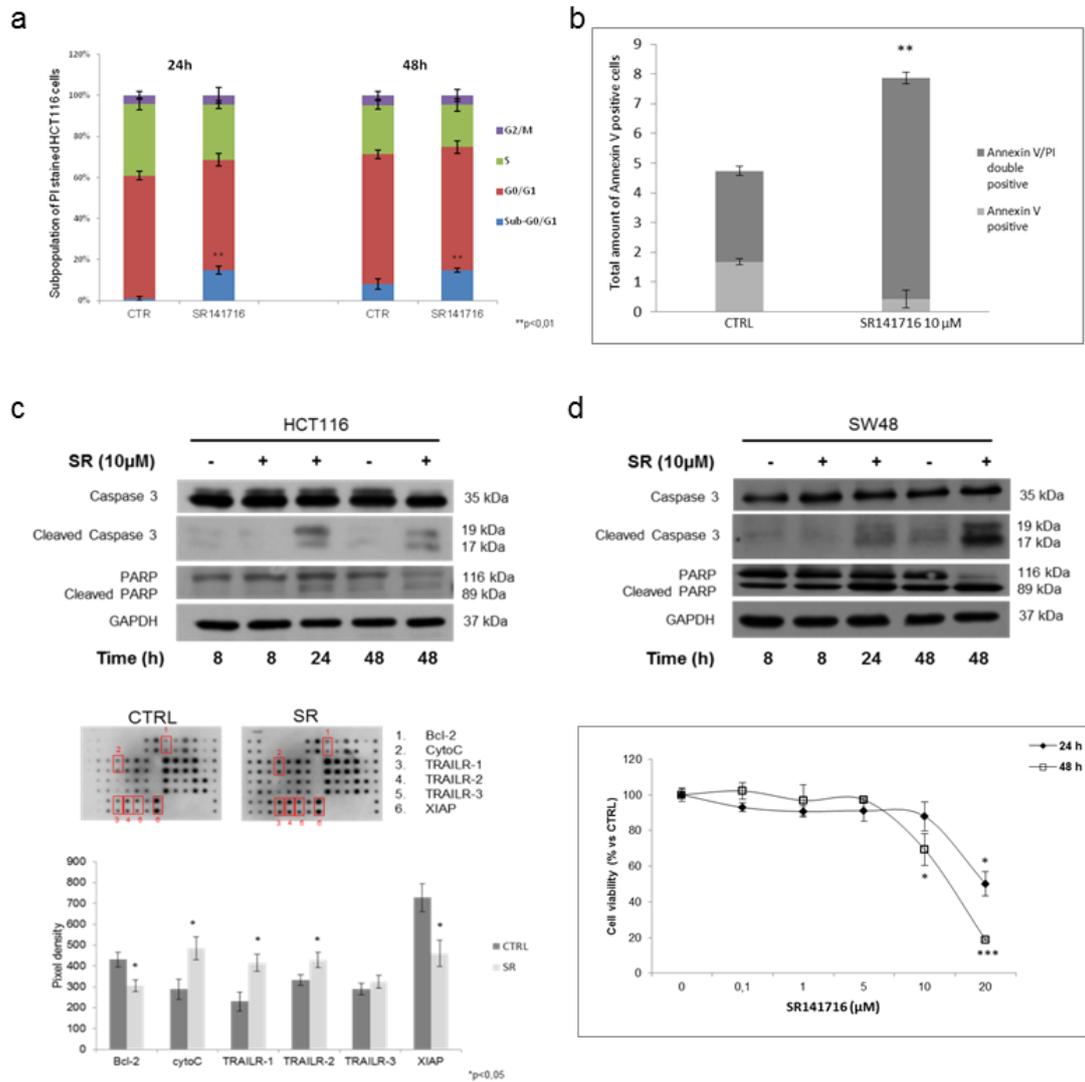
Figure 4. a Cell cycle analysis of PI stained HCT116 cells treated with SR141716 (SR, 10µM). **b** FACS analysis of PI/anti-Annexin V-FITC double stained HCT116 cells untreated or treated for 48 hours with SR141716 (SR, 10µM). **c** upper, representative western blot analysis of caspase 3 and PARP (total and cleaved forms) expression in total protein lysates from HCT116 cells; lower, representative proteomic membrane of Human Apoptosis Antibody Array and relative densitometric analysis performed on total protein lysates from HCT116 treated for 48h with SR 10µM. **d** upper, representative western blot analysis of caspase 3 and PARP (total and cleaved forms) expression in total protein lysates from SW48 cells; lower, MTT assay in SW48 cells treated with indicated doses of SR141716. All experiments were performed in triplicate in at least three times. The results are shown as the mean ± SD (*p<0.05, **p<0.01 and ***p<0.005).

3.2 Cannabinoids inhibit Wnt reporter activity in HCT116 cells.

The downstream effect of Wnt canonical (β-Catenin-dependent) signaling activation culminates with β-Catenin nuclear translocation, where it regulates TCF/LEF transcription factor on target genes promoters. Thus, to evaluate if Met-F-AEA and Rimonabant make β-Catenin unable to activate the transcription of Wnt-regulated genes, analysis of the activation status of reporter genes containing TCF/LEF binding sites was performed through luciferase assay, in HCT116 cells. To evaluate the efficiency of transient transfection, we firstly analyze GFP reporter expression used as positive control. A percentage of about 70% of cells expressing GFP was obtained, indicating a correct and efficient transfection (fig. 5a). Afterwards, in HCT116 cells, luciferase activity was measured through transiently transfection with the reporter containing the TRE for TCF/LEF. As shown in figure 2b, treatments for 24h with Met-F-AEA 10 μM produced only a slight reduction of luciferase activity (about 23%). However, at same time, Rimonabant (10 μM) significantly reduces luciferase activity of about 50% (fig. 5b), showing a more promising activity than Met-F-AEA in Wnt signaling inhibition.

3.3 Rimonabant affects β-Catenin transcriptional activity and sub-cellular localization in HCT116 cells.

The ability of Rimonabant to affects β-Catenin activity was validated analyzing its expression and sub-cellular localization. Immunofluorescence staining of HCT116 cells treated with Rimonabant 10 μM, clearly showed that β-Catenin protein expression results significantly reduced starting from 24h of treatments. Furthermore, analysis of orthogonal projections performed through confocal microscopy, confirm that reduction of β-Catenin transcriptional activity, could be due to Rimonabant-mediated inhibition of nuclear translocation (fig. 6).
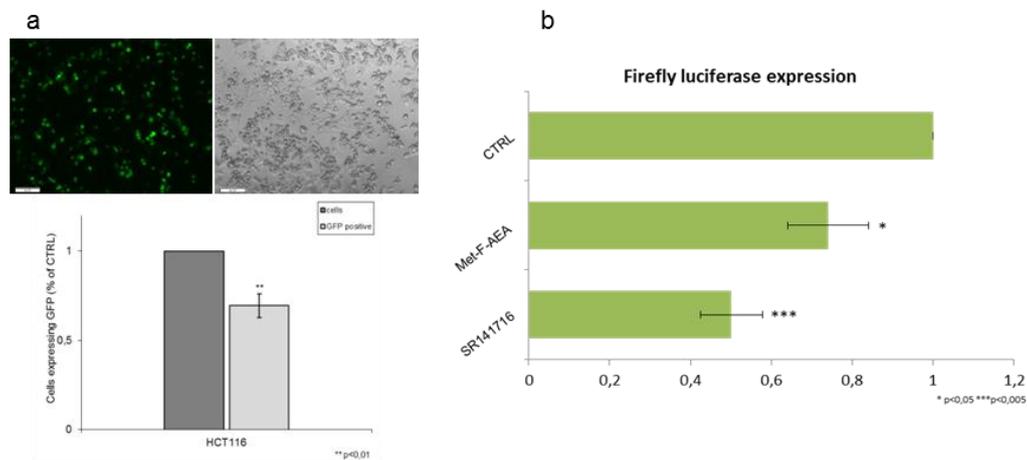
Figure 5. a Upper panel: Fluorescence microphotographs of HCT116 cells transfected with a constitutively expressing GFP reporter construct, used as positive control in the luciferase assays (magnification 10x). Lower panel: efficiency of the transfection procedure was calculated as percentage of green cells *versus* total cells (mean of cellular counts performed in at least 5 microphotographs from 4 independent experiments) **b** Luciferase activity in extracts from HCT116 cells transfected with reporter construct containing the TRE for TCF/LEF (TCF/LEF response element) for 16 hours and treated with SR141716 or Met-F-AEA 10µM or vehicle. The level of luciferase activity was taken as an arbitrary unit. The data are representative of at least three independent experiments where each sample was analyzed in triplicate (mean±SD; *p<0.05, **p<0.01 and ***p<0.005).

Western blot analysis of fractionated cytoplasmic and nuclear protein extract corroborate reduced expression and nuclear localization of β-Catenin, starting from 24h of treatments (fig. 7a). β-Catenin mRNA levels were also reduced by Rimonabant at the same time points (fig. 7b).

As previously described, nuclear translocation of β-Catenin is due to the failure of its degradation in the cytosol. Indeed, β-Catenin destabilization is usually performed by degradation complex containing APC, Axin, CK1 and GSK3-β proteins. The latter two, catalyze β-Catenin phosphorylation on Ser45 and Thr41/Ser37/Ser33 respectively, all tags for proteasome-mediated degradation (Stamos & Weis, 2013). Rimonabant results able to significantly

induce β-Catenin phosphorylation of Ser33/Ser37 residues, starting from 8h and until 48h of treatment with 10 µM (fig. 7c), suggesting that Rimonabant-
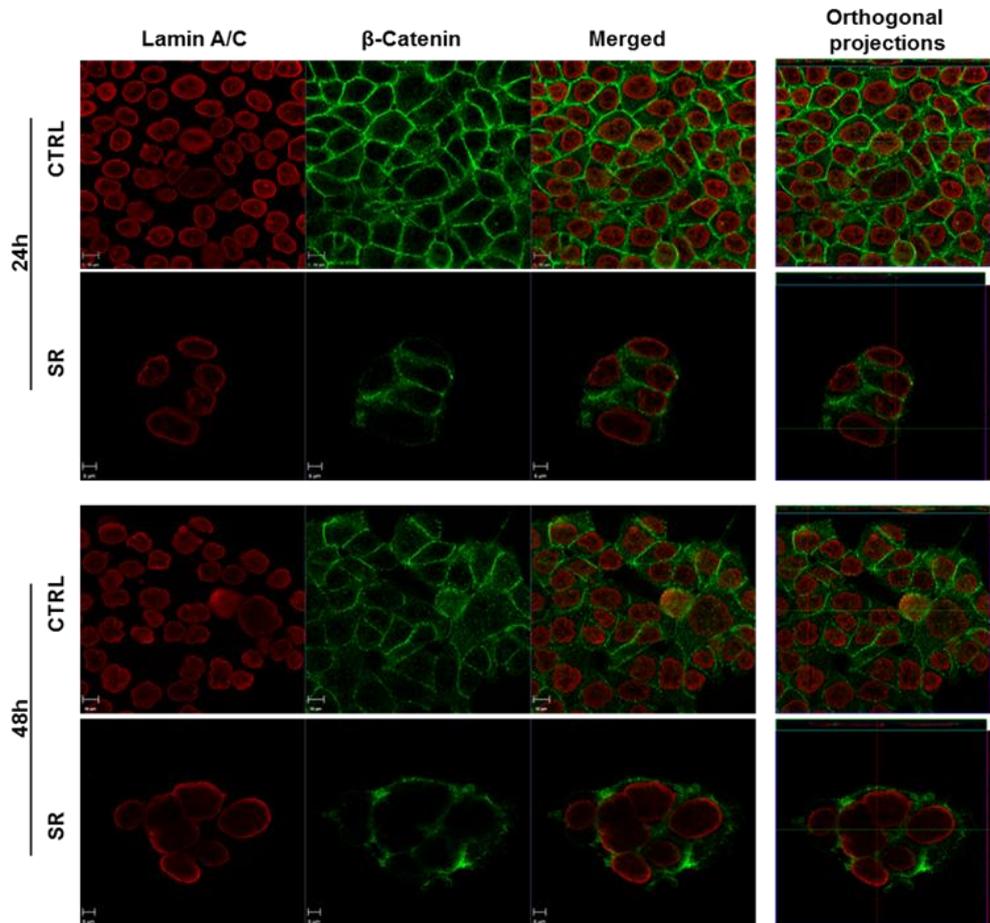

Figure 6. After treatment with SR141716 (SR, 10 µM), HCT116 cells were fixed and stained with anti β-Catenin antibody (green fluorescence) to evaluate subcellular localization. Nuclei were stained with anti Lamin A/C antibody (red fluorescence). In right panels orthogonal view of 0.5 µm thickness in the z plane was reported. The data are representative of three experiments with similar results.

mediated direct inhibition of canonical Wnt pathway, could be ascribable to β-Catenin destabilization.

TCF/LEF activation downstream Wnt signaling, lead to transcription of specific target genes. Among others, Cyclin D1, c-Myc and COX-2 play a key role in colorectal carcinogenesis (Herbst et al., 2014). Then, in order to

confirm canonical Wnt/β-Catenin inactivation, analysis of protein expression of above cited genes was performed through western blot. As shown in figure 3d, in HCT116 cell line, Rimonabant was able to reduce Cyclin D1, c-Myc and COX-2 expression, at the same time points in which a reduction of luciferase activity and β-Catenin nuclear translocation were observed (fig. 7d).
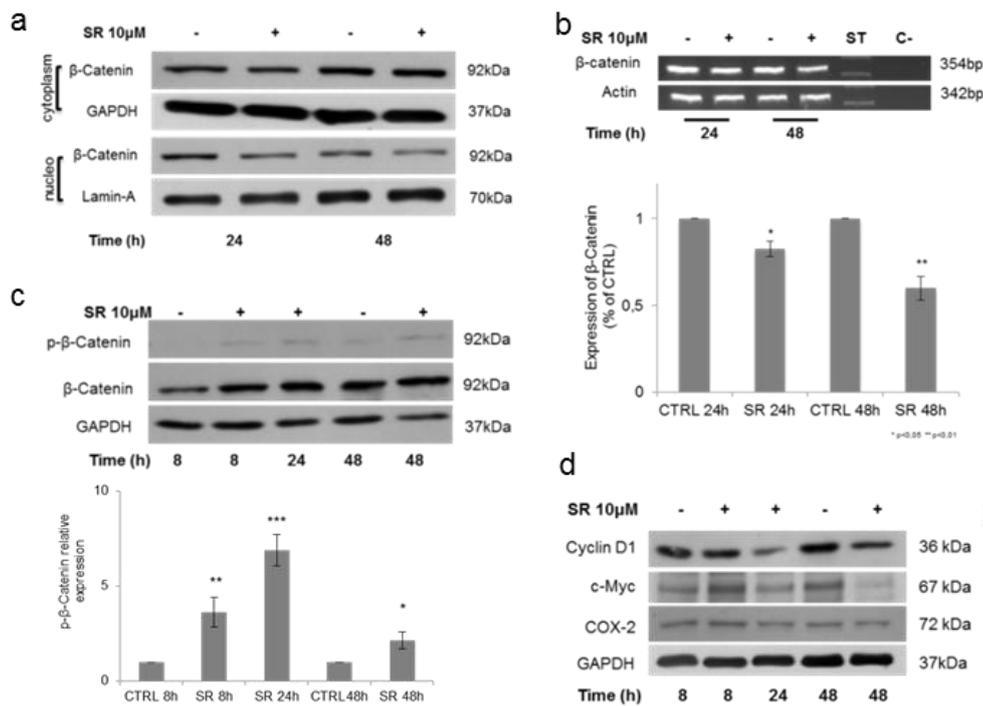

Figure 7. a Western blot analysis of β-Catenin expression in nuclear and cytoplasmic fractionated extracts from HCT116 cells. Cytoplasmic and nuclear amount of β-Catenin were normalized *versus* GAPDH and Lamin A/C respectively. **b** mRNA levels of β-Catenin in HCT116 cells. **c** upper, representative western blot and densitometric analyses of β-Catenin (total and phosphorylated form) expression in HCT116 cells. Lower, the histograms shown represent the densitometric analyses of phospho-β-Catenin expressed as fold change of the total β-Catenin amount and normalized *versus* GAPDH. **d** Western blot analysis of Cyclin D1, c-Myc and COX-2 protein levels in HCT116 cells. GAPDH was used as loading control. The data are representative of at least three independent experiments where each sample was analyzed in triplicate (mean±SD; *p<0.05, **p<0.01 and ***p<0.005).

3.4 Genotype dependence of Rimonabant-mediated Wnt/β-Catenin pathway regulation.

To establish if Rimonabant effects represents a common mechanism in CRC, different cell lines with different genotype, were used. In particular, SW48 cells shows a genetic profile similar to HCT116, carrying β-Catenin gene mutation, APC and p53 wild type genes. Moreover, like HCT116 they present chemoresistant phenotype. Instead, DLD1 and SW620 cell lines do not carry mutations in β-Catenin gene, but are APC and p53 mutant. In addition, they are more sensitive to chemotherapeutics (Data obtained from Colon Cancer Atlas).

First, β-Catenin phosphorylation status was examined. Western blot analysis of total extracts after treatments with Rimonabant 10 μM, showed that the strongest and persistent induction of phosphorylation occurs in SW48, β-Catenin mutated cells, starting from 8h and until 48h of treatments. In DLD1 and SW620 β-Catenin phosphorylation induction, was only slight and not
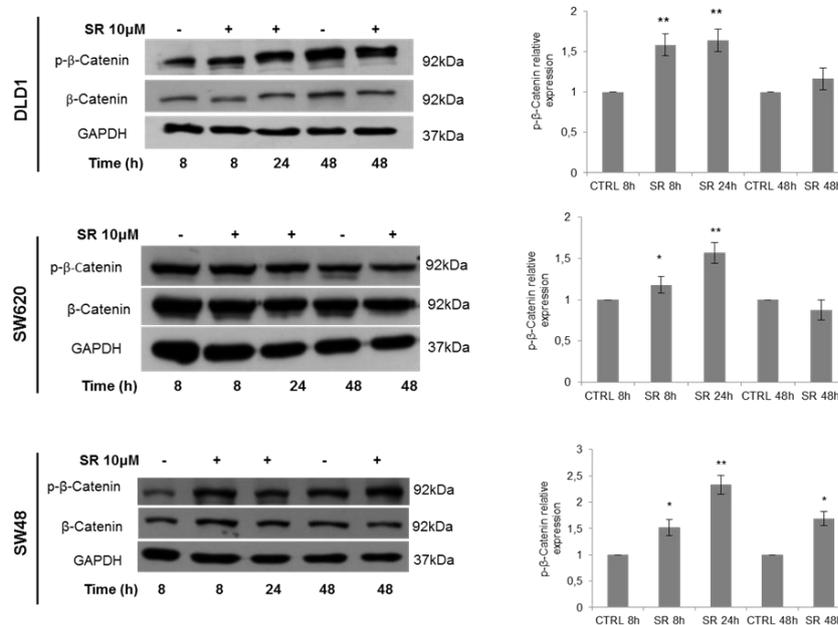
**Figure 8.** Representative western blot and densitometric analysis of β-Catenin (total and phosphorylated form) expression in DLD1, SW48 and SW620 cells treated with SR141716 (SR, 10μM). The histograms shown represent the densitometric analyses of phospho-β-Catenin expressed as fold change of the total β-Catenin amount and normalized *versus* GAPDH. Results are shown as mean ± SD (*p<0.05, **p<0.01).

persistent, compared to β-Catenin mutant cells HCT116 and SW48 (fig. 8).

In canonical pathway (β-Catenin-dependent), interaction of Wnt3 ligand, with Fzd7 receptors and the Wnt co-receptor LRP6 activates the Dishevelled (Dvl3) cytoplasmic phospho proteins, which inhibit the degradation complex consisting of CK1, Axin, APC and GSK3-β, thereby blocking the degradation of β-Catenin and then promoting its nuclear translocation (Anastas & Moon, 2013; Kimelman & Xu, 2006). In HCT116 and SW48 β-Catenin mutant cells, we analyzed the influence of Rimonabant on canonical, β-Catenin-dependent pathway transduction. As shown in western blot panel in figure 5a, both in HCT116 and SW48 cells, the expression of Fzd7 receptor and LRP6 co-receptor were reduced markedly, starting from 24h of treatment with Rimonabant, until 48h. Wnt3 ligand and Dvl3 expression, instead, was reduced starting from 24h for HCT116 and from 8h of treatment in SW48. GSK3-β activity can be inhibited by Akt-mediated phosphorylation at Ser9 (Jacobs et al, 2012). We observed that Rimonabant induced the phosphorylation of GSK3β until 24h in HCT116 and until 48 hours of treatment only in SW48. Finally, a persistent increase of APC levels, were observed only in HCT116 cells (fig. 9a). Substantially, the above described results suggests that in β-Catenin mutant cells Rimonabant is able to directly inhibit canonical signaling across the plasma membrane.

In addition to canonical pathway, Wnt signaling can be transduced through a non-canonical β-Catenin-dependent pathway. The activation of this pathway is triggered by distinct ligands and receptors than canonical way. Among others, Wnt5 is the best know ligand able to activate non-canonical pathway. Wnt5 results frequently downregulated in CRC cells (as in HCT116, SW48 and SW620) due to its promoter methylation (Ying et al, 2008). Wnt5 interacts with ROR2 tyrosine kinase receptor activating actin-binding protein, filamin A, and the JNK signaling pathway (Nomachi et al , 2008; Oishi et al, 2003). In

addition, the non-canonical pathway triggers intracellular calcium flux, associated with CaMKII activation. Moreover, Wnt5 overexpression inhibits
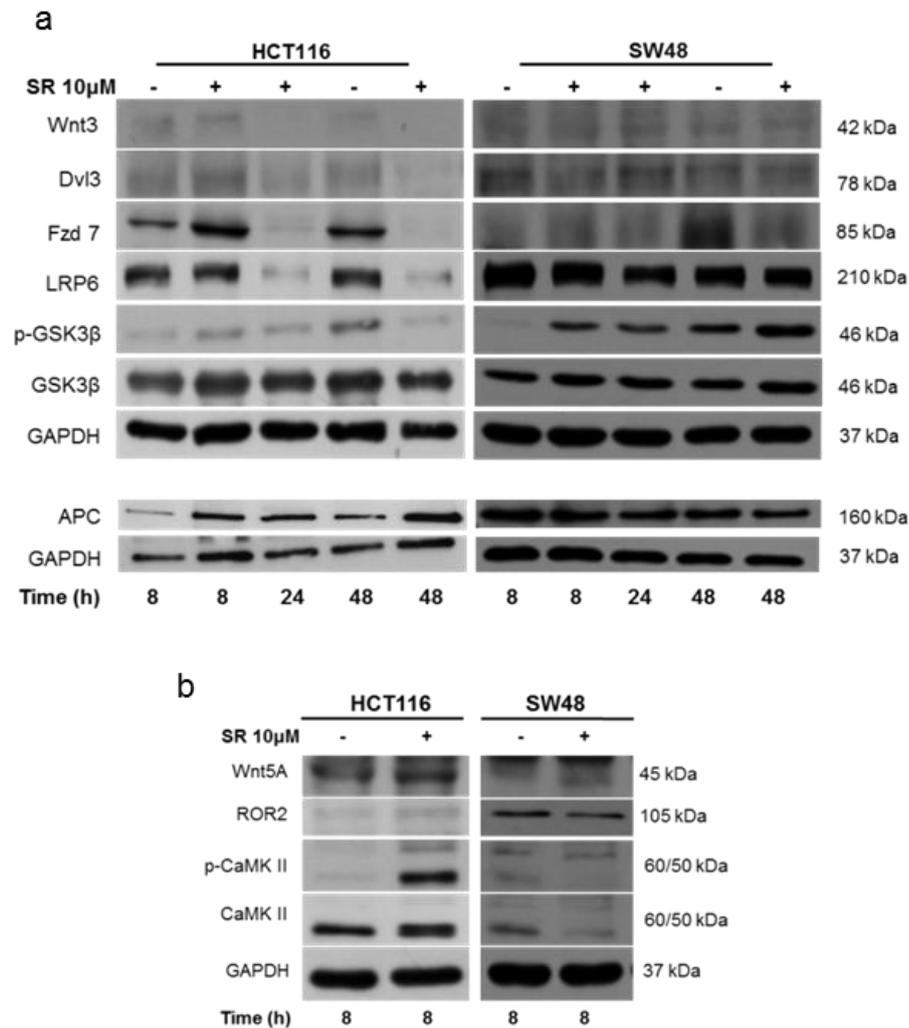
Figure 9. Western blot analysis of protein levels in total lysates from in HCT116 and SW48 cells treated with SR at indicated time points: **a,** canonical pathway: Wnt3, Dvl3, Fzd7, LRP6, GSK3β (total and phosphorylated form) and APC **b,** non-canonical pathway: Wnt5A, ROR2 and CAMKII (total and active form). Blots are representative of at least three indipendent experiments.

canonical pathway and triggers the β-Catenin degradation or the inhibition of TCF/LEF-mediated transcription (Ishitani et al, 2003). To dissect the effect of Rimonabant on non-canonical pathway, western blot analysis was performed.

Rimonabant results able to activate non-canonical pathway, increasing Wnt5 protein levels, Ror2 expression and activation of CaMKII only in HCT116 cells, but not in SW48, after 8h treatments (fig. 9b).

Subsequently, expression of Wnt target genes has been analyzed. Surprisingly, in all the *in vitro* models used, the expression trend of Cyclin D1, c-Myc and COX-2 were similar: starting from 8h of treatments and until 48h, a reduction in protein expression of Wnt-regulated genes was found in both β-Catenin mutant (HCT116 and SW48) and wild type (DLD1 and SW620) cells (fig. 7d and 10).
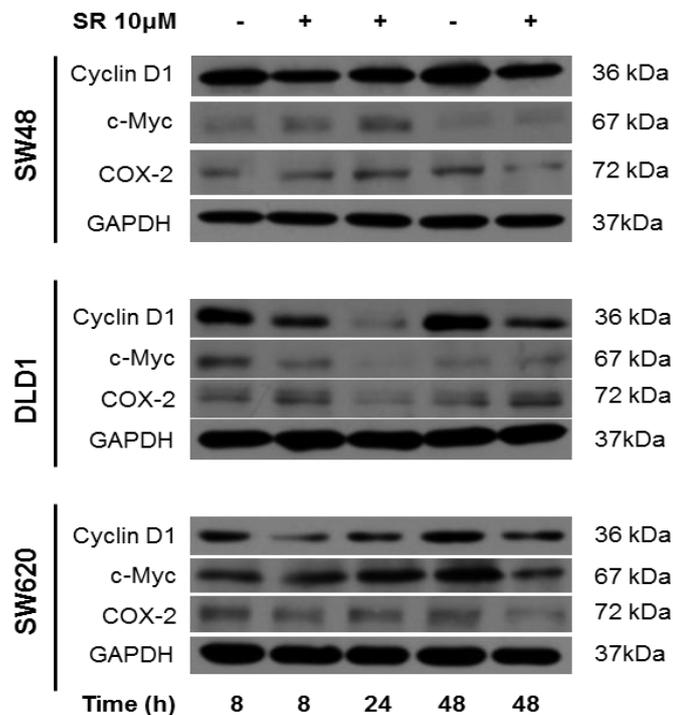
Figure 10. Representative Western blot of Wnt target Cyclin D1, c-Myc and COX-2 protein expression, from SW48, DLD1 and SW620 cells. Blots are representative of at least three indipendent experiments.

Overall, these findings indicate that also in cells were a direct inhibition of canonical pathway was not particular evident (DLD1 and SW620), Rimonabant is able to inhibits downstream Wnt-regulated gene products. This

allow us to hypothesize that an indirect common mechanism mediated by Rimonabant, probably at transcriptional level, leads to downstream inhibition of Wnt signaling.

3.5   p300 is potential binding site for Rimonabant.

To clarify Rimonabant molecular mechanism and then to identify factors potentially able to interact with SR141716, we performed an *in silico* Inverse Virtual Screening testing the case-study compound on a panel of 306 proteins involved in cancer and inflammation events. Briefly, this computational tool allows the analysis of different binding hypotheses between a single ligand and a high number of targets through molecular docking experiments, determining the selection of the most promising ligand−receptor favorite complexes after a normalization of the predicted binding affinities, and successfully directing the subsequent biological assays (Lauro et al, 2012; Lauro et al, 2011).

Among the obtained results, we were intrigued by p300 target at the 3rd position in the final ranking of predicted most affine proteins of SR141716. Specifically, the careful analysis of the sampled docking poses showed a good accommodation of SR141716 in the p300 binding site (PDB code 3BIY), supporting the potential inhibition of the HAT activity exerted by the investigated compound. We found two interesting binding modes in which SR141716 is placed in p300 occupying the Ligand Binding Site (LBD) and exerting both polar and hydrophobic interactions. The analysis of the first pose, associated to the best docking score (ΔG_{bind}=-11.2 kcal/mol), disclosed the arrangement of SR141716 in the deep part of the LBD supported by an edge-to-face π-π interaction between the pyrazole core and the indole moiety in the side chain of Trp1466, and an H-bond with the carbonyl oxygen in the backbone of Leu1398 (fig. 11a). Further polar interactions were established with Ser1396, Asp1399, Ser1400, Arg1410, Gln1455, Lys1456, and

hydrophobic contacts with Tyr1414, Leu1463, Trp1466, Tyr1467 (fig. 11a, c). Another interesting binding mode (ΔG_{bind}=-10.8 kcal/mol) showed the placement of the molecule in a more external part of the binding site, supported by halogen bonds between the dichloro-phenyl part of SR141716 and Arg1410 (fig. 11b), while the edge-to-face π- π interaction between the pyrazole core and Trp1466 was again detected (fig. 11b, d).
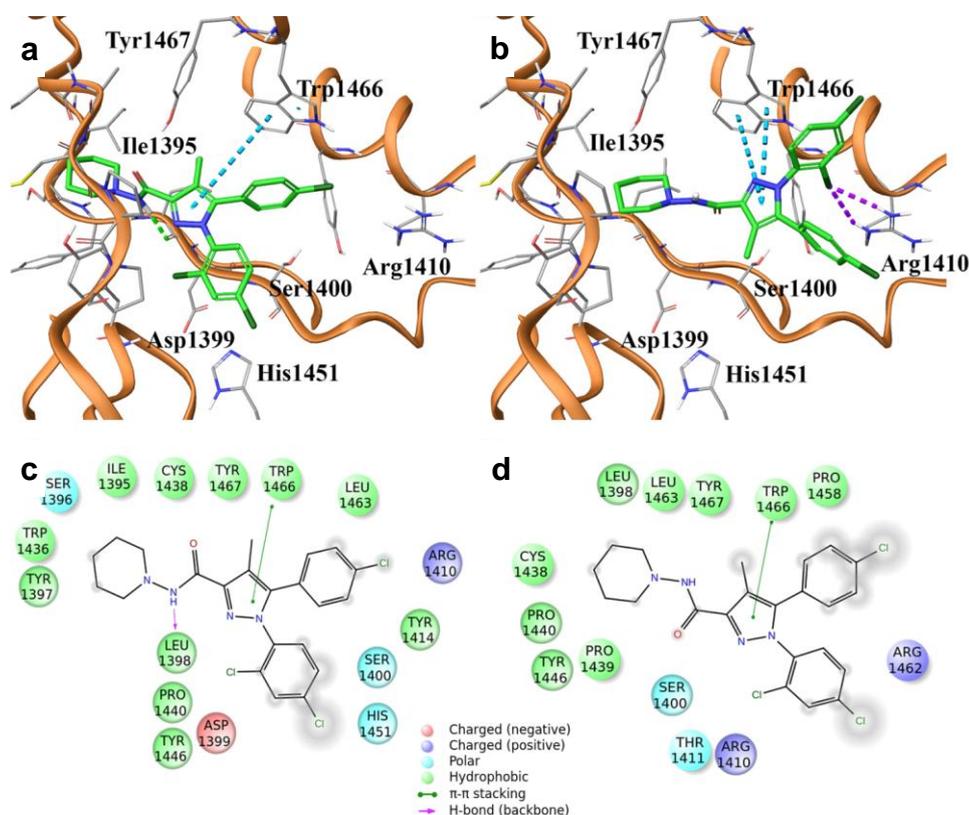
Figure 11. a 3D docking models of SR141716 (colored by atom types: C green, O red, N blue, polar H light gray, Cl dark green) in the binding site of p300 (secondary structure depicted in orange ribbons) and **c** associated 2D interaction panel; **b** alternative 3D docking models of SR141716 and **d** associated 2D interaction panel. Residues in the active site are represented in sticks (colored by atom types: C grey, N blue, O red, S yellow, H light gray). H-bonds ligand/protein interactions are represented in green dotted lines, while π-π interactions are depicted with cyan dotted lines.

3.6   Rimonabant inhibits p300 histone acetyltransferase activity.

Results from Inverse virtual screening, strengthened our previous hypothesis of Rimonabant-mediated transcriptional regulation. C-terminal domain of β-Catenin interacts, in the nucleus, with various chromatin remodelling protein. Among others, p300 and CBP Histone Acetyl Transferases (HATs) interact with β-Catenin and TCF transcription factor on Wnt-Response Elements (WRE). This interaction activates transcription of several Wnt/β-Catenin target genes, due to intrinsic HAT activity of p300/CBP, which results in rapid acetylation of histone H3 and H4 (Bordonaro & Lazarova, 2016; Mosiman et al, 2009).

Since Inverse Virtual Screening assay identificate p300 catalytic domain as specific binding site for Rimonabant, we evaluated p300 HAT activity through fluorimetric cell-free assay. Using anacardic acid (12,5 µM) as positive control, we asses assay efficiency. In a dose-dependent manner, starting from 5 µM, Rimonabant results able to significantly reduce histone H3 acetylation as reflected by Coenzime A-SH (CoA-SH) reduced production and then reduced fluorescence emission (fig. 12).
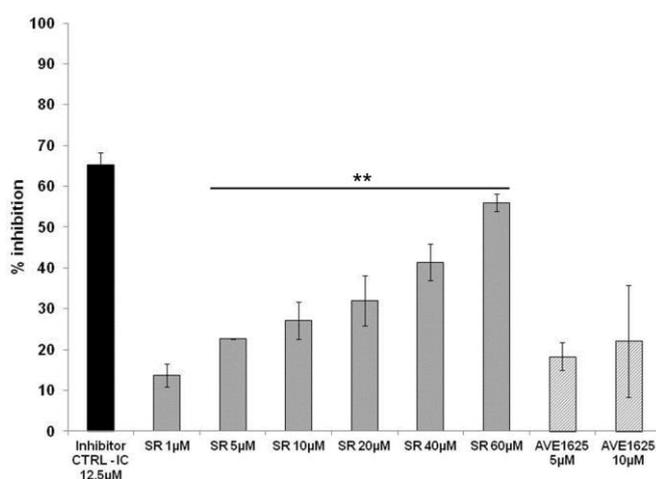
Figure 12. a Kat3B/p300 histone acetyltransferase activity fluorimetric assay performed with recombinant p300 in the presence of SR141716, AVE1625, anacardic acid (used as inhibitor control) or vehicle alone. Results were expressed as means ± SD of 3 independent experiments performed in duplicate and reported as percentage vs the vehicle control (ANOVA. **P < 0.01 vs

To verify if Rimonabant ability to reduce p300 HAT activity could be linked to CB1 receptor inhibition, we used in parallel another CB1-selective inhibitor, AVE1625 (also known as Drinabant). As shown in figure 12, AVE1625 was not able to reduce histone H3 acetylation, indicating that, even if further experiments are required, Rimonabant-mediated HAT inhibition could be CB1-indipendent mechanism.

To confirm p300 HAT inhibition, analysis of global histone H3 and H4 acetylation status, was performed using colorimetric assay on histone extracts from HCT116, DLD1 and SW48 treated with Rimonabant (10 µM) or vehicle alone, for indicated time points. In HCT116 cells both histone H3 and H4 acetylation were strongly and significantly reduced starting from 4h of treatments with Rimonabant. In SW48 and DLD1, instead, only slight reduction of both modifications was found between 4h and 8h of treatments in DLD1 and after 6h of treatments in SW48 (fig. 13). Western blot analysis of protein total extracts substantially confirmed results obtained with colorimetric assay, showing a similar trend expression of acetylated histone H3 and H4 (fig. 13)
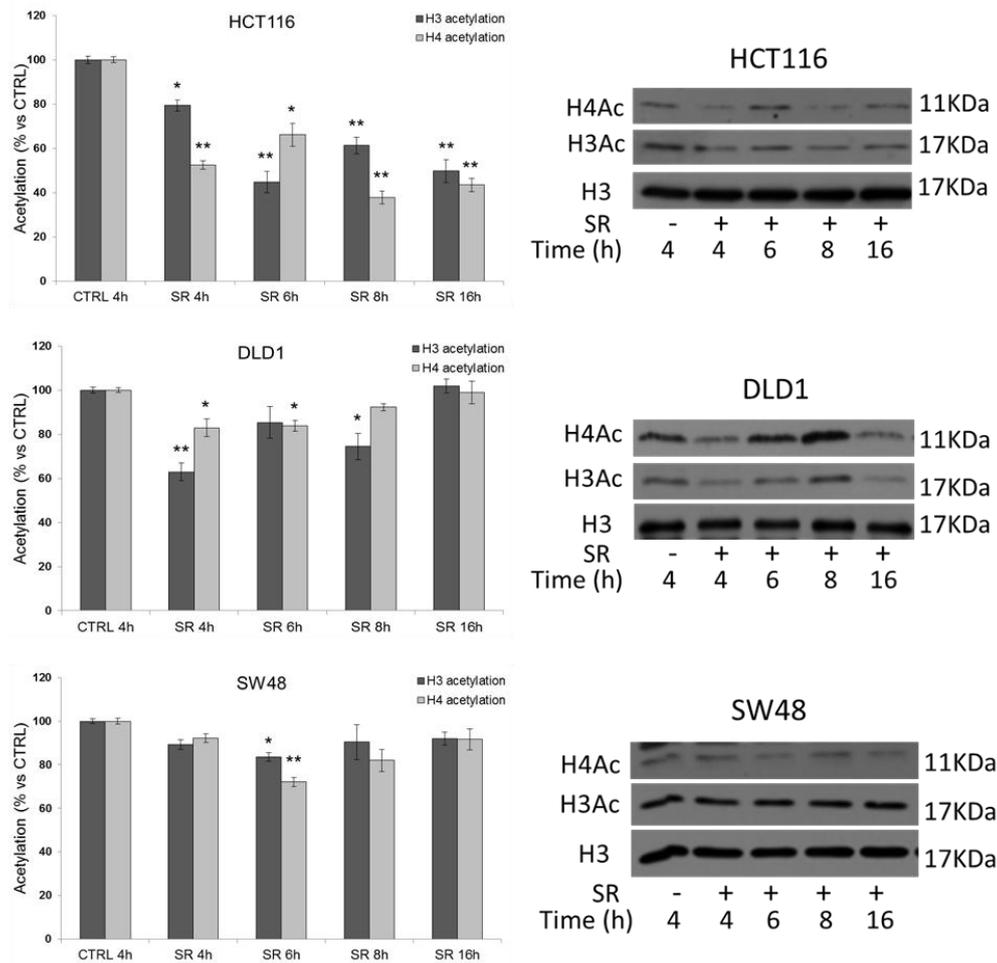
Figure 13, Left histograms, quantification of histone-H3 and histone-H4 total acetylation with a colorimetric assay in histone extracts from HCT116, SW48 and DLD1 cells treated with SR10μM; right panels, representative western blot analysis of histones extracts from HCT116, DLD1 and SW48 cells. Filters were probed with H4 acetylated (AcSer1, AcLys5-8-12) or H3 acetylated (N-terminus) antibodies; Histone H3 were used as loading control. Panels are representative of 3 separate experiments. Results were expressed as means ± SD of 3 independent experiments performed in duplicate and reported as percentage vs the vehicle control (ANOVA, *p<0.05, **P < 0.01 vs control).

3.7 Rimonabant reduces CRC growth and Wnt/β-Catenin signaling *in vivo*.

To evaluate *in vivo* Rimonabant efficacy, we also tested its effects in a subcutaneous (s.c.) HCT116 xenograft model. Tumor cell suspension was injected s.c. into 20 female SCID mice and when the tumor reached approximately the size of 50-70 mm^3, 10 mice in the treated group received each the peri-tumoral injection of Rimonabant (0,07 mg/Kg/dose), while 10 mice in the control group received vehicle alone. The tumor sizes have been recorded on the first day of Rimonabant treatment (day 0) and bi- or three-weekly at the indicated time points. The intratumoral injections of the drug were then repeated three times a week for 6 weeks. All of the mice in vehicle (control) group developed tumors beyond 2,0 cm^3 on average by day 42. In contrast, the mice in Rimonabant group developed much smaller tumors (figure 14a). In particular, by treatment day 42, ANOVA analysis indicates a significant smaller tumor size in treated group compared with animals in the control group (p<0.001) (figure 14b).

Furthermore, after 42 days from treatment beginning, excised tumor sections were analyzed for β-Catenin localization in cellular compartments through immunofluorescence staining with specific antibodies for β-Catenin and for Lamin A/C (green and red fluorescence, respectively in figure 13c). The confocal microscopy demonstrated that in tissue sections from treated mice β-Catenin localized mainly in the cytoplasm whereas nuclear staining was almost devoid of specific β-Catenin signal (figure 14c).

Finally, western blot analysis of total extracts from tissue specimens demonstrated that, despite the awaited tumor samples heterogeneity, the amount of p-β-Catenin, clearly detectable in the treated xenografts, was lost in control tumors and both Cyclin D1 and c-Myc protein levels were reduced (figure 14d).
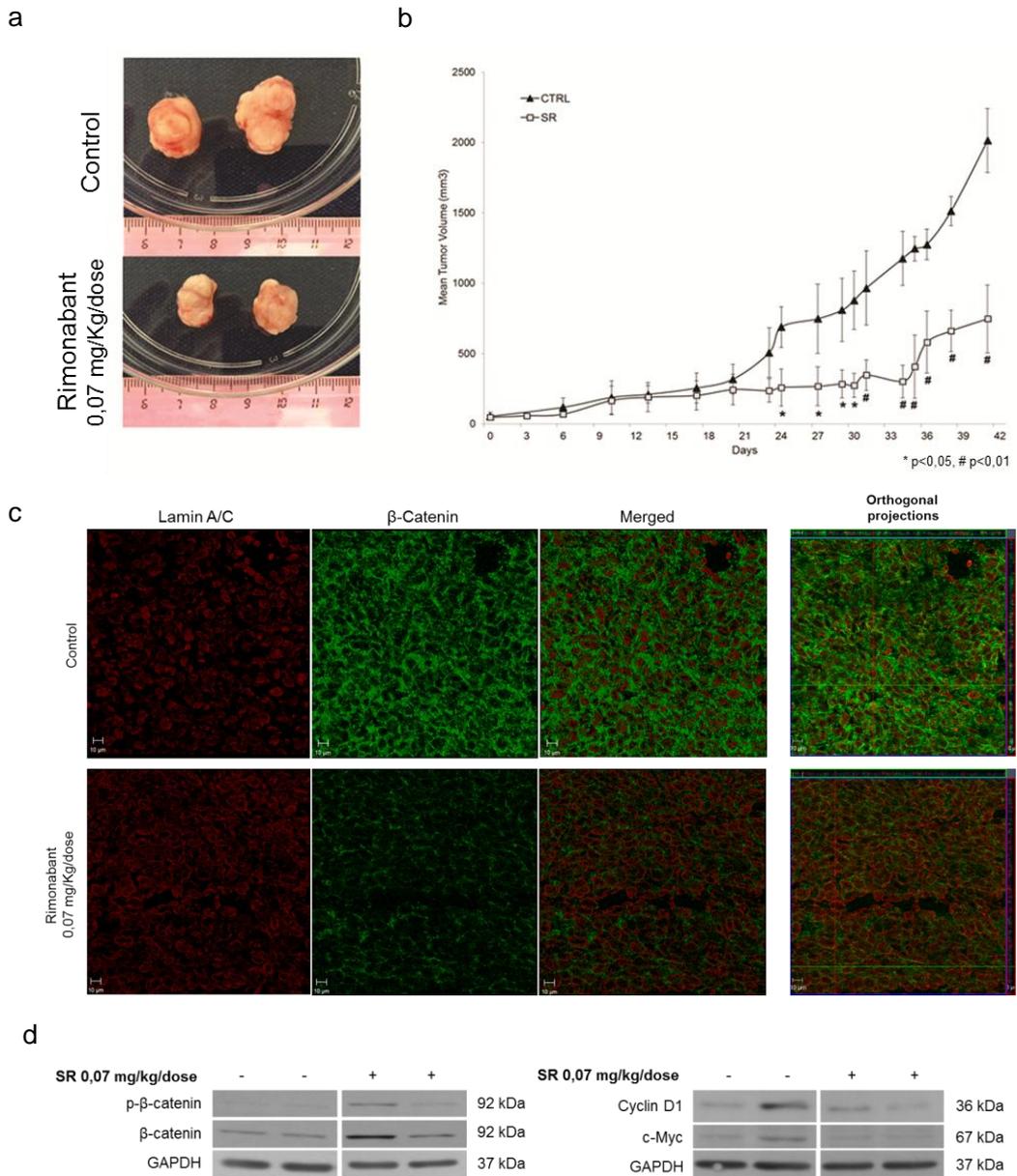
Figure 14. a Representative growth of HCT116 xenograft in control (upper panel) and in treated groups (lower panel) at day 42. **b** Tumor volume growth curve after peri-tumoral injection of SR141716. Growth retardation by the compound was statistically significant for all time points labeled with * (p < 0.05) or with # (p<0,01). **c** Immunofluorescence staining of HCT116 xenografts tumor sections (10µm) performed for Lamin A/C (red fluorescence) and β-Catenin (green fluorescence) localization. Data are representative of at least three sections from each control and treated tissue sample. **d** Western blot analysis of total and phosphorylated β-Catenin (left panel), Cyclin D1 and c-Myc (right panel) in total lysate from resected tumor tissues. Results are representative of at least four samples analyzed in two independent experiments**.**

3.8 Rimonabant control cancer stemness and chemoresistance in HCT116 cells.

A growing number of evidence, indicates that Wnt hyperactivity is closely related to stem-like phenotype and a large numbers of markers helps in the identification, isolation and targeting of CSCs (Kemper et al, 2010; Vermeulen et al, 2010).

Our results, showed that Rimonabant is able to inhibit Wnt signaling. To establish if this compound can control cancer stemness, FACS analysis of CD133/CD44 double positive population was performed. After 48h hours, Rimonabant significantly and strongly reduces CD133/CD44 double positive HCT116 cells (fig. 15a). Together with CD44, Lgr5 is Wnt-regulated genes, CSCs markers specifically associated to 5-FU chemoresistance in colon cancer patients (Hsu et al, 2013). In parallel with reduction of CD133 and CD44 expression, Rimonabant reduces Lgr5 expression (fig. 15b), suggesting its potential role in cancer stemness control.
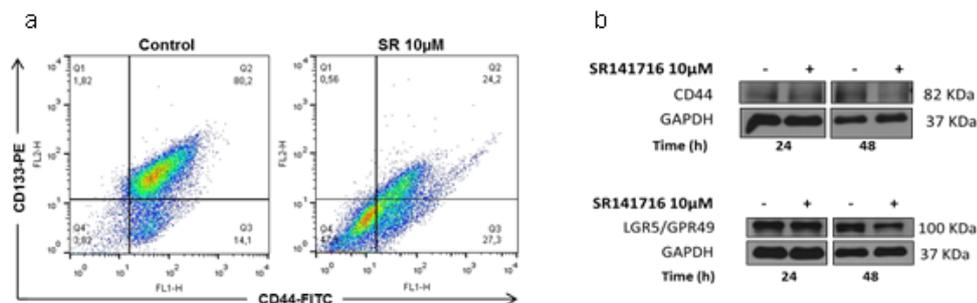
Figure 15. a FACS analysis of CD133-PE/CD44-FITC double stained HCT116 cells after treatment for 48h with SR 10μM. **b** Western blot analysis of CD44 and LGR5 in total protein lysates from HCT116 cells. Data are representative of at least three independent experiments.

Despite in the last decades great advances has been obtained in cancer management, the complete eradication is still an open challenge. Relapses onset is largely attributed to the presence of chemoresistant CSCs, refractory
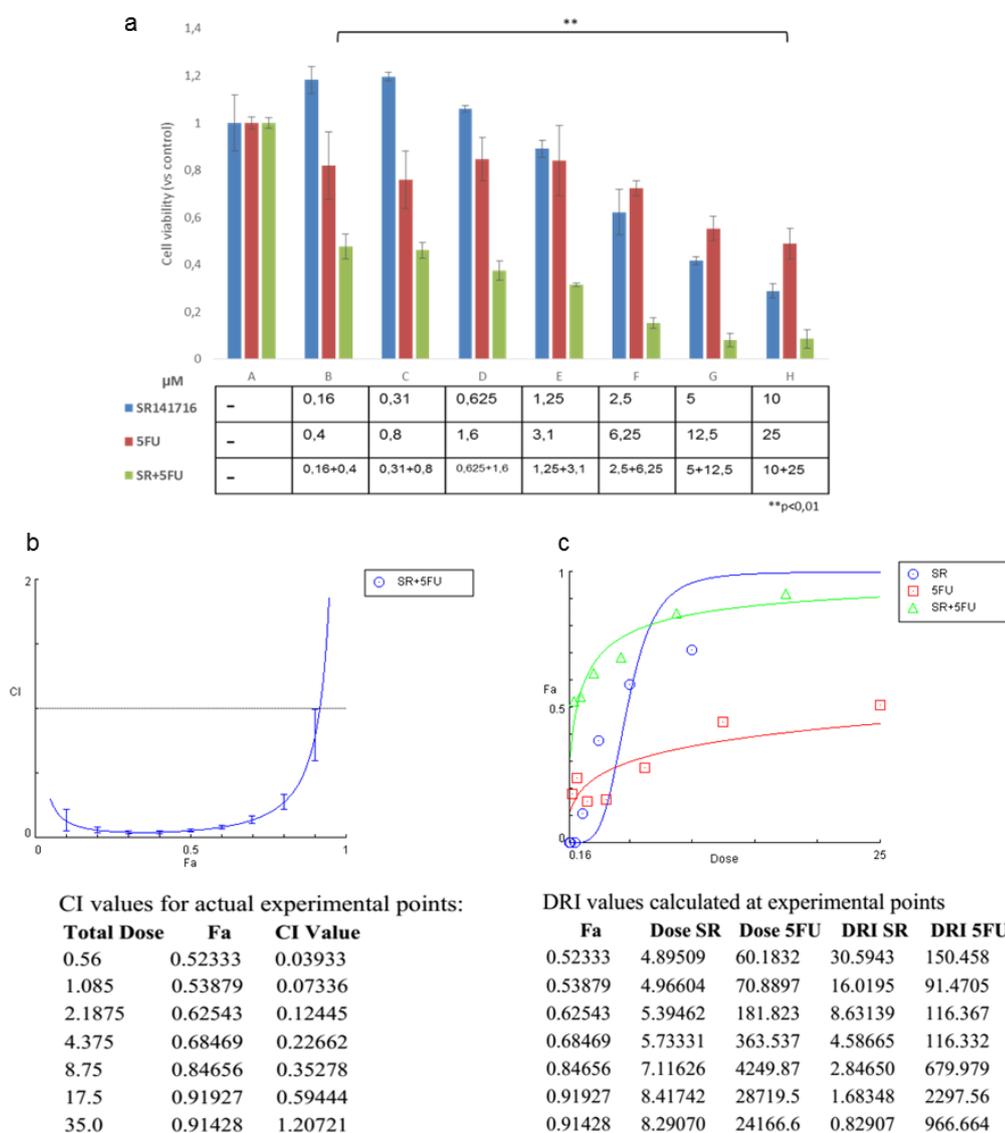
Figure 16. a MTT assay performed in HCT116 cells treated with indicated concentrations of SR or 5-FU alone or in combination; data are expressed as means ± SD of 3 independent experiments performed in triplicate and reported as percentage vs the vehicle control (**P < 0.01 vs control). **b** Combination Index plot (Fa-CI plot) obtained with Compusyn software entering the Fraction affected (Fa) at each dose of the drugs alone or in combination, at constant ratio, in three independent experiments (upper) and Fa-CI table from Compusyn related to experimental points (lower). **c** upper, Compusyn Dose Reduction Index plot (Fa-DRI); lower, Fa-DRI table for experimental points, for each drug in their combination.

to conventional chemotherapy (Zeuner et al, 2014). To evaluate if Rimonabant could ameliorate the antitumor effects of 5-Fluorouracil, one of the most used chemotherapeutics in colon cancer treatment, MTT assay was performed in combined treatments, in dose-dependent manner.

Specifically, 24h co-treatments of Rimonabant with dose range of 0,16 - 10 µM in combination with 5-FU with dose range of 0,4 - 25 µM, were performed in HCT116 cells. As indicated in figure 16a, combination of this two compunds significantly ameliorates the effect of 5-FU, starting from non-active single doses of 0,16 µM and 0,4 µM of Rimonabant and 5-FU, respectively. Moreover, analysis of pharmacologic interaction with Compusyn software, reported a Combination Index ≤ 1, starting from 0,16 µM and 0,4 µM and until 5 µM and 12,5 µM of Rimonabant and 5-FU, respectively, indicating a synergistic interaction (fig. 16b). In figure 15c, Dose Reduction Index of both compounds obtained with Compusyn software, are reported for each combination.

3.9   Cell death induction in colon cancer stem cell line GTG7.

As described in materials and methods, GTG7 cells are patients derived spheroidal cultures, stable transfected with Wnt-TOP-GFP reporter. Since Wnt activity correlates with cancer stemness (Vermeulen et al, 2010), in this culture it's possible to distinguish between CSCs (identified as TOP-GFP^{high} or Wnt^{high}) or differentiated tumor cells (TOP-GFP^{low} or Wnt^{low}), thereby taking into account of tumor heterogeneity. To evaluate Rimonabant-mediated cell death induction on CSCs, caspase-3 activity was measured with FACS-based CaspGlow active staining kit, gating on 10% of TOP-GFP^{high} (CSCs) and, in same experiment, on 10% TOP-GFP^{low} (differentiated tumor cells). FACS analysis of GTG7 cells treated for 24h with Rimonabant 5-10-15 or 20 µM revealed that Rimonabant significantly activates caspase-3 both in Wnt^{low} differentiated tumor cells (in a more pronounced manner) and in Wnt^{high}
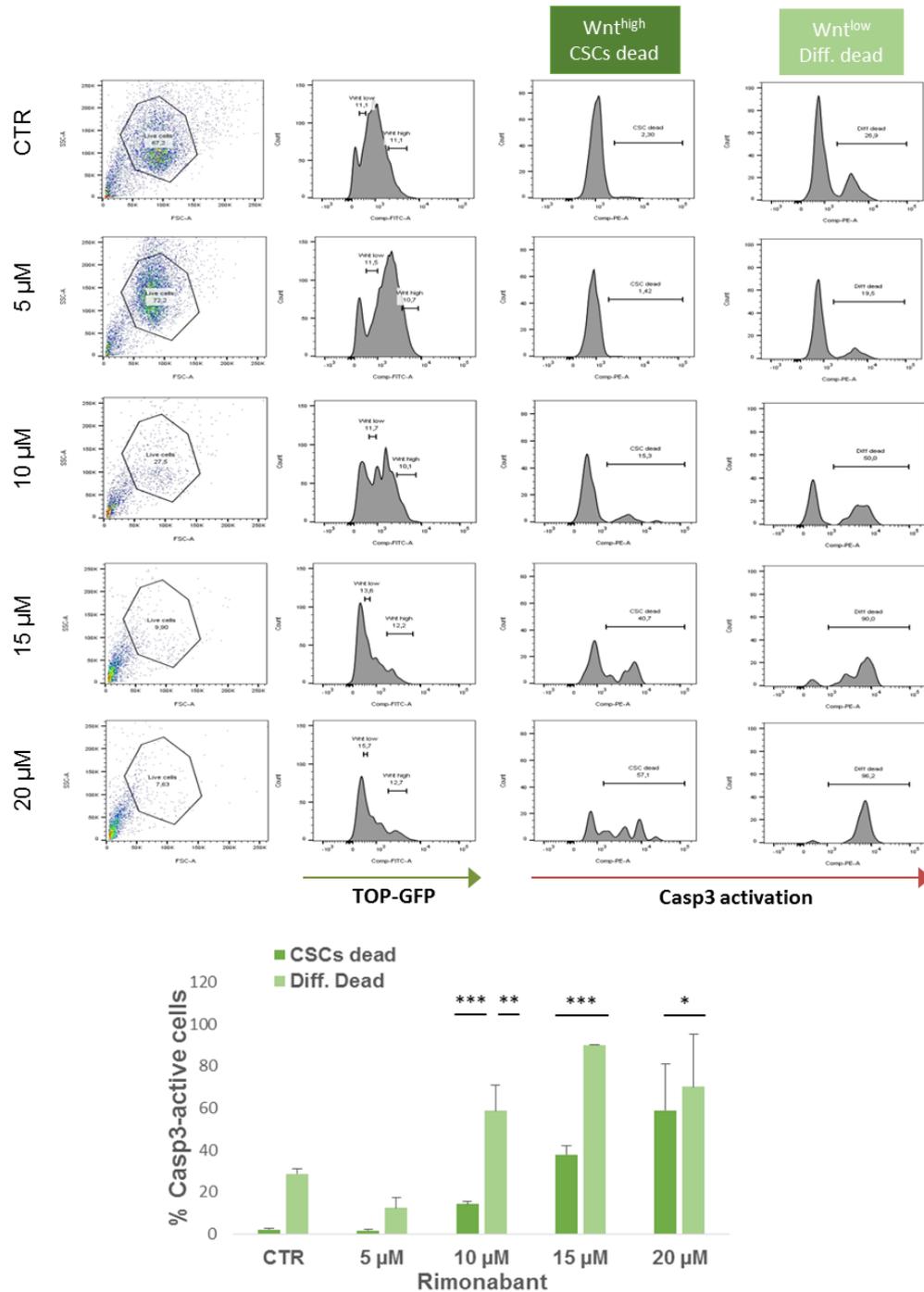
Figure 17. Representative histograms (upper panel) and bar histogram (lower) of Caspase 3 activation in GTG7 cells treated for 24h with Rimonabant or veichle alone at the indicated doses. Caspase 3 (PE quantification) was analyzed gating on 10% of TOP-GFP^{high} (Wnt^{high}) cells, corresponding to CSCs, and on 10% TOP-GFP^{low} (Wnt^{low}) cells, corresponding to differentiated tumor cells. Data are expressed as mean ± SD of at least three independent experiments in duplicate (*p<0.05, **p<0.01, ***p<0.005).

CSCs, in a dose-dependent manner, starting from 10 µM (fig. 17). This result reveals for the first time the ability of Rimonabant to induce cell death mechanisms in chemoresistant and high tumorigenic colorectal CSCs population. Furthermore, in a same manner, a conspicuously DNA fragmentation supports Rimonabant-mediated cell death induction in GTG7 (fig. 18).
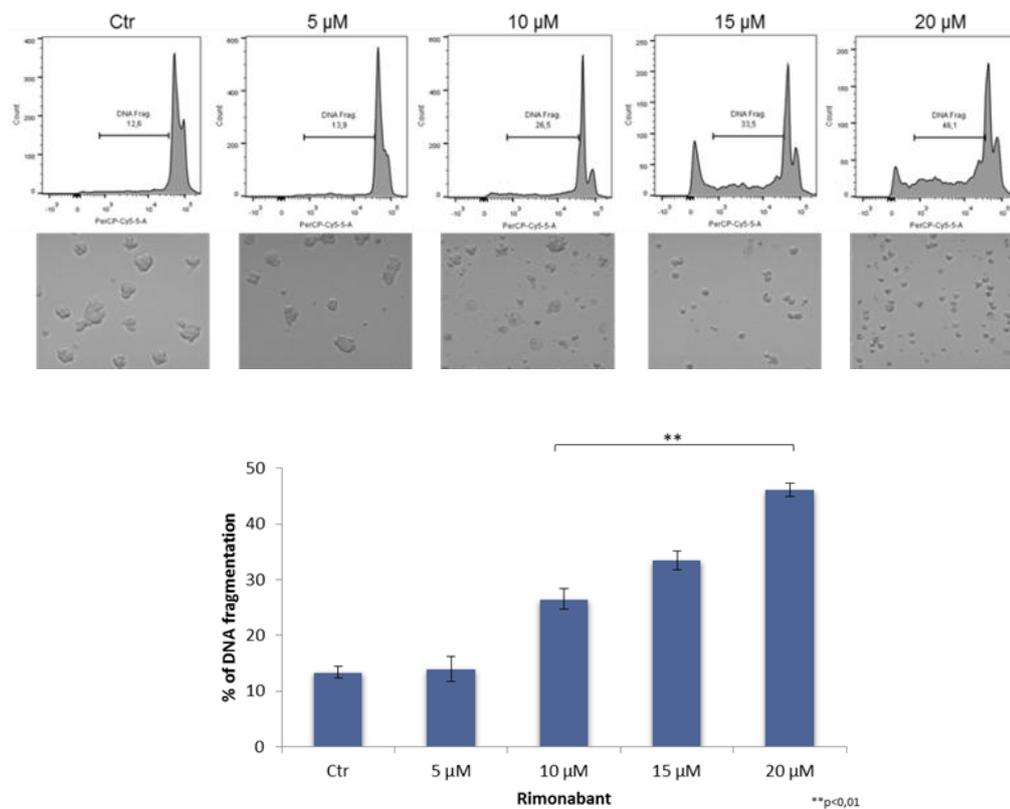
Figure 18. Representative histograms and images (upper panel) and bar histogram (lower) of DNA fragmentation amount in PI-stained GTG7 cells, treated for 24h with Rimonabant or veichle alone at the indicated doses. Data are expressed as mean ± SD of at least three independent experiments (**p<0.01).

3.10 Reduction of CSCs survival in long-term cultures.

Given to their chemoresistance and high tumorigenicity, CSCs are certainly associated to tumor recurrence (Zeuner et al, 2010). Thus, development of

novel strategies to overcome CSCs long-term survival and spreading is essential for complete eradication.
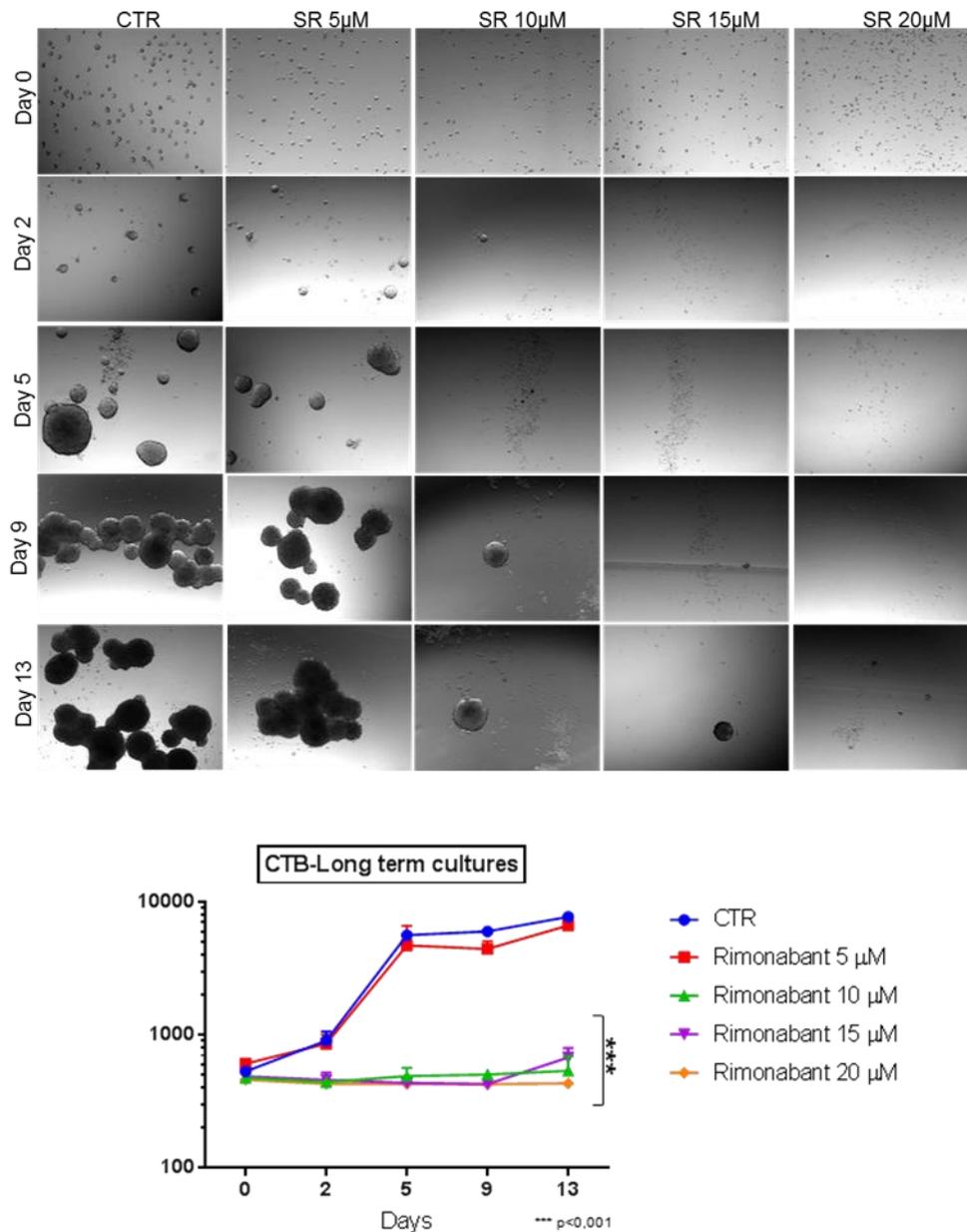
Figure 19. upper panel, Representative images of GTG7 clones after 24h of treatment with Rimonabant (or veichle control) starting from day 0 (corresponding to the end of treatments) and until day 13. Growth of spheroidal clones was monitored in three independent experiments in triplicate. Lower, Cell Titer Blue (CTB) colorimetric assay in GTG7 treated for 24h, as described. Data are expressed as mean ± SD of at least three independent experiments in triplicate (***p<0.005).

In the light of results obtained, Rimonabant effects on GTG7 clonogenicity was performed. To this aim, GTG7 were treated with dose range 5-20 µM for 24h. At the end of treatments Rimonabant was re moved from culture medium. The cells from each replicate were collected and seeded as spheroids in non-adherent conditions. Through Cell Titer Blue colorimetric assay, viability of spheroids was monitored starting from day 0 (which coincides with the end of treatments) for total 13 days. As clearly shown in figure 19, Rimonabant strongly reduces GTG7 survival: with 10 and 15 µM, the appearance of vital clones were detected only after 9 days. After 13 days, at 20 µM dose vital clones were not identified, suggesting a probable excessive toxicity of this dose. Substantially, reduction of GTG7 survival in long-term cultures supports Rimonabant ability of cancer stemness control.

3.11 Rimonabant does not improve Oxaliplatin and 5-Fluorouracil effects in GTG7 cells.

Previous results in HCT116 cell line, show that a synergistic interaction exists between Rimonabant and 5-FU. Since CSCs are highly chemoresistant, FACS analysis of caspase-3 activation was performed in GTG7, on Wnt^{high} CSCs and Wnt^{low} fractions. To this aim, GTG7 were pre-treated for 6h with Rimonabant 10 µM. At the end of pre-treatments, 25 µM of Oxaliplatin or 5-FU were added for total 24h. As shown, at these concentrations Rimonabant reduces the efficacy of Oxaliplatin and produces only a slight but non-significant improvement of 5-FU efficacy (fig. 20). Even if further experiments are required to establish the type of pharmacologic interaction, this result could suggest an antagonistic interaction, particularly with Oxaliplatin.
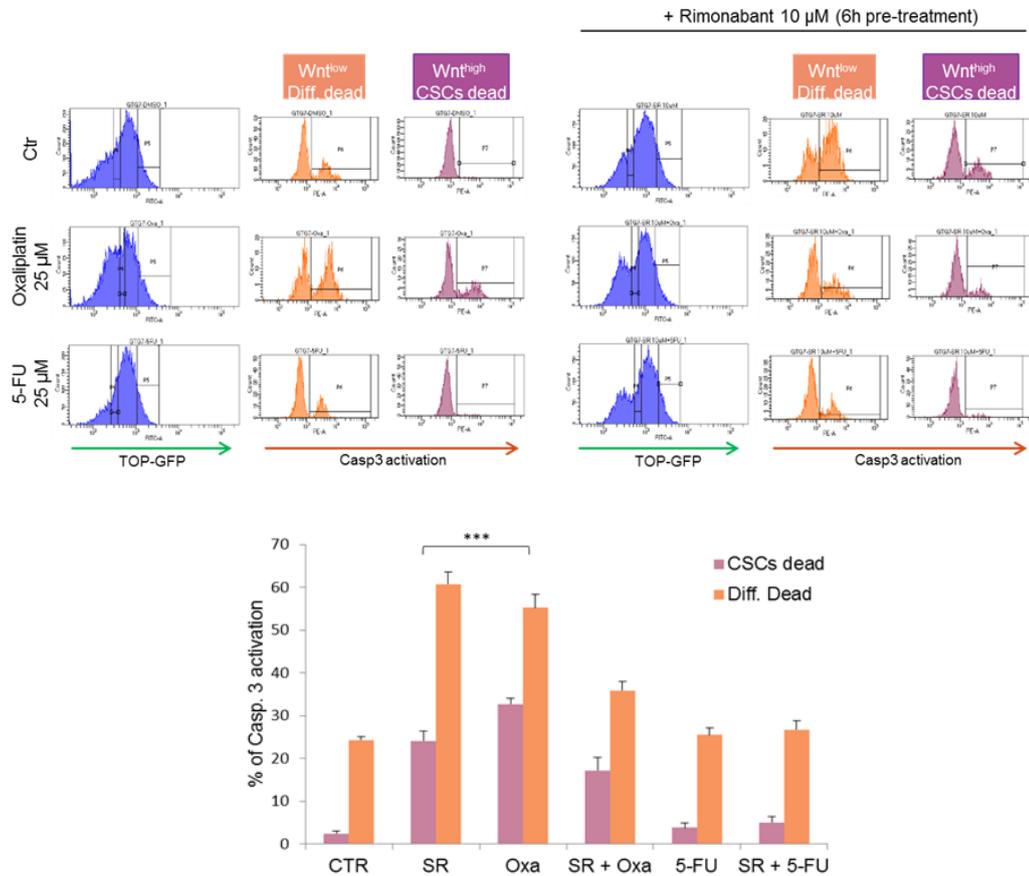
Figure 20. Representative histograms (upper panel) and bar histogram (lower) of analysis of Caspase 3 activation in GTG7 cells treated with single or combined compunds Rimonabant 10μM, 5-FU 25μM, Oxaliplatin 25μM or veichle alone. Caspase 3 (PE quantification) was analyzed gating on 10% of TOP-GFP^{high} (Wnt^{high}) cells, corresponding to CSCs, and on 10% TOP-GFP^{low} (Wnt^{low}) cells, corresponding to differentiated tumor cells. Data are expressed as mean ± SD of at least three independent experiments in duplicate (***p<0.005).

3.12 Rimonabant shows no toxicity against normal colon human organoids.

Encouraging results obtained *in vivo*, *in vitro* and for the first time in isolated primary colon CSCs, strongly suggest that Rimonabant could be a novel lead compound in treatment of high malignant colorectal cancer. Since that ideal therapeutic strategy consists of selective compounds toward cancer cells, with lowest toxicity against healthy tissues, evaluation of Rimonabant effects on normal colon was performed in wild type normal colon human organoids cultures.

As described in material and methods, normal colon organoids derived from patients, were cultured in matrigel and treated for 24h with Rimonabant 10, 15 and 20 µM, corresponding to the most active concentration in GTG7. At the end of treatments (fig 21a), for each replicate matrigel was destroyed and removed. Crypts were collected, disaggregate and stained with PI for FACS evaluation of DNA fragmentation status. Surprisingly, FACS analysis of cells derived from Rimonabant treated organoids showed the same percent of fragmented DNA compared to control organoids, also at 20 µM dose, suspected of extreme toxicity against GTG7 (fig 21b). Finally, we performed clonogenic assay on normal colon organoids. After 24h of treatments at indicated doses, Rimonabant was removed, crypt were collected, diluted and seeded again in new matrigel. Crypts were counted on day 0 (corresponding to end of treatments) and after 7 days. Ratio of clones number on day 7 respect to clones number on day 0, indicates that Rimonabant don't reduces clonogenicity of wild type normal colon organoids (fig. 21c). On the other hand, at 15 µM dose, Rimonabant seems to induce clonogenicity. Further experiments are required to clarify if this last result could be due to Rimonabant direct effect on normal colon differentiation.
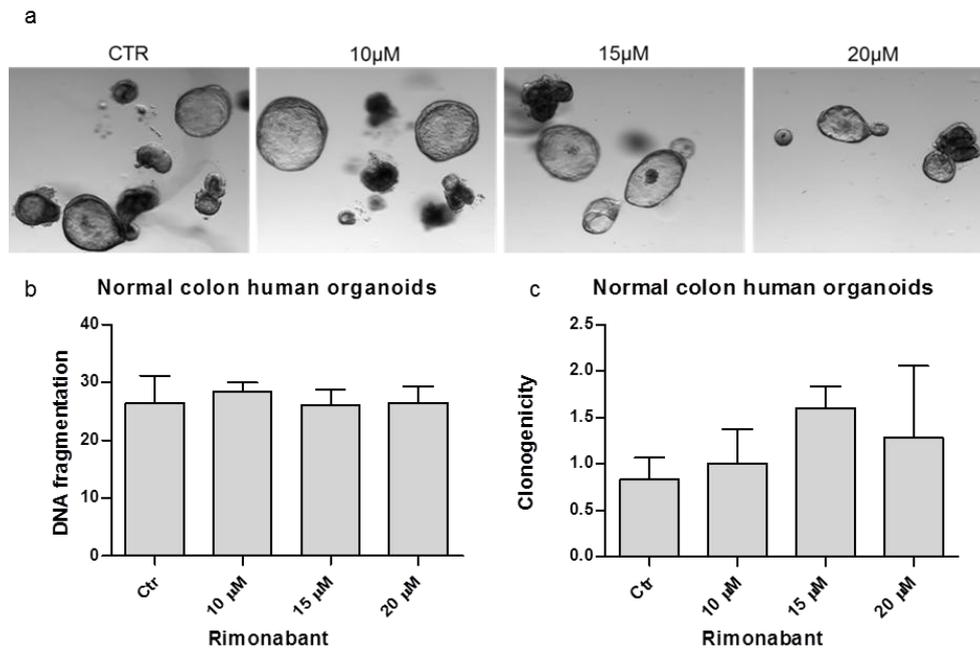
Figure 21. a Representative images of normal colon human organoids cultured in matrigel and treated for 24h with Rimonabant or veichle alone at the indicated doses. **b** Analysis of DNA fragmentation amount in PI-stained cells derived from normal colon human organoids treated for 24h with Rimonabant or veichle alone at the indicated doses. **c** Analysis of normal colon human organoids clonogenicity after treatments with Rimonabant or veichle alone at the indicated doses. Results represents the ratio of number of clones on day 7 *vs* number of clones on day 0 (corresponding to the end of treatments). Data are expressed as mean ± SD of two independent experiments.

CHAPTER IV

DISCUSSION

Despite in the last decade the improvement of colon cancer management increases patient's life expectancy, eradication of high malignancy forms, then metastatic and drug resistant phenotypes, remain a still open challenge to contrast disease relapses. Thus, discovery and development of new drugs aimed to ameliorate therapeutic protocol for advanced malignancy are urgently needed.

It has become clear that CRC is a heterogeneous disease, both at intratumoral and intertumoral level (Punt et al, 2016). This increases difficulties in its management and, therefore, development of personalized medicine protocols based on molecular subtype, is the best solution for an ideal therapy. To date, understanding of molecular mechanisms responsible for chemosensitivity, influences clinical decision about the use of EGFR inhibitors (e.g. cetuximab or panitumumab), small molecules targeting BRAF or combined use of tyrosine kinase (TKI) and histone deacetylase (HDACi) inhibitors (Hertzman Johansson & Egyhazi Brage, 2014; LaBonte et al, 2011; Bardelli & Siena, 2010). However, discovery and characterization of novel prognostic biomarkers need to be improved.

Recently, Guinney and colleagues (2015), proposed a novel gene expression–based subtyping classification system for CRC. They identified four Consensus Molecular Subtypes (CMSs), with different signatures. CMS2

(canonical) is the largest subgroup (about 37%) presenting Myc and Wnt pathway hyperactivation. This result confirmed that Wnt/β-Catenin pathway plays a pivotal role in the onset and progression of CRC and the study of its intricate regulation is now emerging as a promising field to identify potential target of intervention for CRC treatment

Generally, Wnt pathway seems to be cell and context specific and the Wnt targetome regulates several functions in the cellular context, both in healthy and cancer tissues (Anastas & Moon, 2013; Vlad et al, 2008). Despite the difficulties in the control of this complex signaling, several compounds able to inhibit Wnt activity are under development in anticancer therapies. In an ongoing clinical trial, LGK974 (also known as WNT974) porcupine inhibitor, which blocks the palmitoylation and secretion of Wnt ligands (Liu et al, 2013), is used in triple combination with LGX818 and Cetuximab in BRAF[V600]-mutant metastatic CRC (#NCT02278133). Many other clinical trials are currently ongoing. Of note two non-steroidal anti-inflammatory drugs (NSAIDs) are able to inhibit Wnt signaling: sulindac, Dvl inhibitor currently in phase II trials and celecoxib, β-Catenin inhibitor in COX-2-dependent and –independent manner (Takebe et al, 2015; Lee et al, 2009). Moreover, inhibitors of CBP/β-Catenin interaction, in particular ICG-001 and the second-generation compound PRI-724, also received great interest. PRI-724 antitumor action was evaluated in phase Ib trial, in combination with FOLFOX6 protocol (#NCT0132405) in metastatic CRC patients.

Intriguingly, some authors reported that cannabinoid compounds are able to modulate Wnt/β-Catenin pathway in cancer. Specifically, anandamide (AEA) activates non-canonical Wnt5-mediated signal, inhibiting cholangiocarcinoma growth (DeMorrow et al, 2008) and in breast cancer cells, met-F-AEA inhibits (TCF) responsive element activation, reduces β-catenin protein levels and downregulates mesenchymal markers expression (Laezza et al, 2012). Moreover, many authors demonstrated that some cannabinoids, inhibit

gliomagenesis, targeting glioma stem cells and inducing their differentiation (Aguado et al, 2007; Nabissi et al, 2015). In addition, Sharma and colleagues (2014) reported that cannabis extracts with high CBD concentration, was able to control prostate cancer stem cells, inhibiting spheroids growth, *in vitro*. These observation strongly suggest a potential role of cannabinoids in Wnt-related mechanisms, such as cancer stemness.

For decades, despite some unresolved disputes, endocannabinoid system modulators have gained increasing attention not only for their effects against cancer-related symptoms (such as anti-inflammatory, pain reliever or antiemetic action), but also as anticancer agents in many tumour types, including colon cancer (Velasco et al, 2016; Maida et al, 2016). Many reports indicate that cannabinoid compounds are able to reduce progression of CRC *in vivo* in the azoxymethane (AOM) induced ACF model in mice and to improve the efficacy of chemotherapeutic drugs used in the clinical practice (Gazzerro et al, 2010; Santoro et al, 2009; Gustaffson et al. 2009; Izzo et al, 2008). In addition, Proto and colleagues, in 2010, demonstrated that increased availability of cannabinoids, of both exogenous and endogenous sources, in CRC cells induced up-regulation of CB1-receptor expression by co-localization of PPARγ and RXRα at the promoting region and increased the expression of ER-β, thus suggesting a potential epigenetic modulation in cannabinoids-mediated antitumor effects.

Previous works from our group reported that an antagonist/inverse agonist of CB1 receptor, Rimonabant is able to exert antitumor action in different cancer models (Ciaglia et al, 2016; Malfitano et al, 2012). Of note, In CRC cell lines (DLD-1, CaCo-2 and SW620 cells), Rimonabant produced mitotic catastrophe and modulated the expression of Cyclin B1, PARP-1, Aurora B and phosphorylated p38/MAPK and Chk1, improving the efficacy of Oxaliplatin (Gazzerro et al, 2010; Santoro et al, 2009).

In this work, we evaluated antitumor action of four different cannabinoids compounds, in high malignant human CRC cells HCT116, expressing APC and BRAF wild type and harboring β-Catenin mutation (loss of phosphorylation site S45), KRAS^{G13D} and PIK3CA^{H1047R} activating mutations that confers maximal resistance to Cetuximab (Jhawer et al, 2008). The most active compounds were met-F-AEA and in particular Rimonabant, that in our model was also able to induces G0/G1 accumulation and apoptosis. In the light of previous reports, the main goal of the project was to test the hypothesis that antitumor effects of both CB1 agonist and antagonist in CRC could be due to direct modulation of Wnt/β-Catenin pathway. Inhibition of TCF/LEF reporter gene, highlighted for the first time the ability of Rimonabant, more than met-F-AEA, to contrast Wnt hyperactivation in our *in vitro* model of colorectal cancer. Moreover, in HCT116 Rimonabant inhibits β-Catenin nuclear translocation, probably because of its cytosolic destabilization, evidenced by the increased phosphorylation, known to be tag for proteasomal degradation. An indirect evidence of reduced β-Catenin nuclear activity, was obtained analyzing expression of TCF/LEF-controlled gene products, Cyclin D1, COX-2 and c-Myc, well know genes involved in CRC carcinogenesis. Results showed that in HCT116 cells Rimonabant strongly reduces expression of these genes. Interestingly, as described above COX-2 inhibitors (e.g. NSAIDs drugs) are currently under investigation as Wnt/β-Catenin pathway inhibitors. Transcription of COX-2 gene is controlled by several consensus sequences in the promoter region, including TFC/LEF responsive elements. Moreover, prostaglandin E2 (PGE2), a COX-2 product, reduces β-Catenin phosphorylation and increases its nuclear localization. Finally, Celecoxib, was found to inhibit both c-Met and Wnt activity in CRC cells (Castellone et al, 2005; Tuynman et al, 2008; Nuñez et al, 2011). Some results showed that the endogenous cannabinoid AEA inhibits the growth of CRC cell lines

expressing moderate or high COX-2 levels but not of cells with very low COX-2 expression. In these models, the AEA induced cell death seems mediated via its metabolism by COX-2, rather than degradation into arachidonic acid and ethanolamine (Patsos et al, 2005). This allow us to speculate that Rimonabant-mediated inhibition of Wnt signaling could be ascribable not only to direct inhibition of CB1 receptor, but probably to other CB1-independent mechanisms, such as COX-2 inhibition. Of course, further investigations will clarify this hypothesis.

As discussed, our principal model HCT116 cell line, arbor mutation of β-Catenin gene (loss of phosphorylation site S45), rather than APC. Since that this genotype represents only a small percentage of CRC, we analyzed Rimonabant effects on Wnt signaling in three other CRC *in vitro* models, aimed to establish if the observed effects were related to specific genotype. We chose SW48 cells, displaying genetic profile similar to HCT116, harboring loss of phosphorylation site of β-Catenin, and presenting APC wild type gene. Moreover, both HCT116 and SW48 cells are highly insensitive to some chemotherapeutic drugs. In human CRCs, the loss of function of APC is mainly ascribable to truncated mutations rather than hypermethylation of the APC gene promoter (Zhang et al, 2009). Several reports indicated that APC regulates β-Catenin degradation complex in different way and cancer-specific APC truncation did not prevent completely β-Catenin phosphorylation, but inhibit β-Catenin ubiquitination and degradation, with final effect of still reduced nuclear translocation (Wang et al, 2014; Yang et al, 2006). Thus, we used DLD1 and SW620 cell lines, β-Catenin wild type cells, presenting APC truncation. In addition, they are more sensitive than SW48 and HCT116 to chemotherapeutics. As expected, analysis of β-Catenin phosphorylation status, revealed that the strongest and persistent induction arise in β-Catenin mutant cells, HCT116 and SW48. In both two latter cell lines, moreover, direct

inhibition of canonical Wnt signal through plasma membrane was found. In addition, only in HCT116 cell line, Rimonabant increases the activity of the non-canonical Wnt/β-Catenin pathway through up-regulation of Wnt5A and ROR2 receptor and activation of CaMKII. Even if further investigation are needed to explain why non-canonical pathway activation occurred only in HCT116 cells, the results seem also suggest that Rimonabant could be able to upregulate the expression of both APC and Wnt5A.

In the light of the role of APC truncation in CRC, as described above, the finding that Rimonabant reduces the expression of the Wnt-regulated genes, Cyclin D1, COX-2 and c-Myc with similar trend in all the models used, it is not so surprising. Indeed, this result, it's in agreement with reports from Wang and colleagues (2014), which indicate that in DLD1 and SW620 cells, were APC truncation occurs, the weak induction of β-Catenin phosphorylation, did not ruled out its reduced nuclear activity.

Encouragingly, our data demonstrated for the first time the *in vivo* efficacy of Rimonabant in reducing the HCT116 xenograft growth. In tissue specimens from xenografts, despite the awaited tumor samples heterogeneity, the evidence of an increased expression of p-β-Catenin and down-regulation of c-Myc and Cyclin D1 seems to represent a very encouraging validation of the Rrimonabant efficacy in tumors harboring β-Catenin mutation. These data show, for the first time, enough direct evidence of the inhibition of the canonical Wnt/β-Catenin pathway and of β-Catenin target genes by cannabinoid compounds in human CRC.

Results from cell-free Inverse virtual screening study, suggested that Rimonabant shows high affinity to HAT catalytic domain of p300. Since p300 play a key role in β-Catenin transcriptional machinery, this finding corroborated our hypothesis of a Rimonabant-mediated transcriptional mechanism and led us to explore this novel role for this cannabinoid

compound. Our results, confirmed that Rimonabant inhibits HAT-p300 activity, as also evidenced from reduced histone H3 and histone H4 acetylation, in particular in HCT116 cells.

Discovery of this unexplored novel role for Rimonabant, takes significance that is even more important if we consider some aspects: to date, selective p300 inhibitors were not identified, but in CRC both CBP-specific inhibitor (ICG-001) and p300/CBP non-selective inhibitor (C646) inhibit Wnt signaling. Of note, in HCT116 cells these two compounds regulate Wnt-target genes (such as c-Myc and Cyclin D1) with similar trend (Gaddis et al, 2015). Some evidence indicate that specific p300- or CBP-β-Catenin interaction, may differentially regulate apoptosis and proliferation of colon cancer cells (Bordonaro & Lazarova, 2016; Lenz & Khan, 2014). However, the precise differences between p300- or CBP-mediated Wnt-regulation is a still open question and further investigation will help to elucidate CBP- or p300-mediated changes in colonic neoplastic phenotype. Despite this, as witnessed by the fact that they are under investigation in ongoing clinical trials, p300/CBP inhibitors remain promising compounds in colon cancer treatment, able to inhibit Wnt signalling and, in addition, to control cancer stemness in several tumor types (Takebe et al, 2015).

Supported by encouraging results, as next step we tested the hypothesis that Rimonabant could control colon cancer stemness. As widely reported, Wnt and c-Myc hyperactivity, contrasted by Rimonabant, are clearly markers of CSCs. However, tumor heterogeneity implies that only a small subset of tumor cells retains tumorigenic ability, while a largest part differentiated in tumor cells that lost the ability to initiate cancer. The so-called CSCs, are certainly associated to tumor recurrence given their high chemoresistance to the large part of chemotherapeutics (Zhao, 2016; Paldino, 2014; Zeuner et al, 2014; Todaro et al, 2010). Wnt hyperactivation in CSCs is associated with specific markers such as CD133, CD44 and Lgr5. Firstly, in line with our previous

findings, we found that Rimonabant reduces CD133/CD44 HCT116 double stained subpopulation and downregulates Lgr5 expression. As CD44, Lgr5 is Wnt-regulated gene associated to 5-FU chemoresistance in colon cancer patients (Hsu et al, 2013). Gazzerro and colleagues (2010) demonstrated that Rimonabant ameliorates Oxaliplatin effect in CRC cell, *in vitro*. Here we showed that this cannabinoid compound, in parallel with Lgr5 reduction in HCT116, was able to produce strong synergistic interaction with 5-Fluorouracil, to date one of the widely used drugs in CRC management.

Vermeulen and colleagues, in 2010, developed an *in vitro* model of primary CSCs in which it's possible to take into account of tumor heterogeneity, monitoring Wnt activity. In this model, Rimonabant confirmed its ability to control cancer stemness, inducing strongly activation of caspase 3, then cell death, both in differentiated tumor cells (characterized by Wnt-low activity) and in CSCs (defined as Wnt-high active cells). Certainly, this result indicated that Rimonabant is not selective toward CSCs, but the observation of a strong reduction of CSCs survival in long-term cultures, allow us to confirm for the first time Rimonabant ability in colon cancer stemness control. Unfortunately, in primary CSCs, Rimonabant did not resulted able to ameliorate nor Oxaliplatin neither 5-Fluorouracil effects. Probably, this latter result, could be due to the high chemoresistance of CSCs.

Since Wnt/β-Catenin pathway regulates both normal and cancer tissues homeostasis, its targeting in CSCs could be a risk against normal tissues. For this reason, safely eradication of CSCs and, generally, of cancer cells, need to be improved by discovery of selective drugs. In recent years, development of *ex vivo* cultures "organoids", in which material from patients can be cultured *in vitro*, retaining both architecture and heterogeneity of original tissue, pioneered the better understanding of both tumor biology and normal tissue homeostasis. These models are currently used for a wide spectrum of application, such as personalized medicine, living biobanks, genetic analysis,

but also drug discovery (Ohta & Sato, 2014; Leushacke & Barker, 2014). In our previous work, we reported the antiproliferative effect of Rimonabant in glioma cell line and primary cells from patients, without significant toxicity in Normal Human Astrocyte (NHA), thus demonstrating moderate selectivity toward glioma cells, *in vitro* (Ciaglia et al, 2015). Here, for the first time, we demonstrated that in normal colon human organoids (wild type organoids that recapitulate, with high fidelity, normal colon epithelium) Rimonabant did not shows toxicity or clonogenicity reduction in normal cells, also at higher doses. To date, many reports tried to elucidate distribution of receptors, ligands and enzymes of endocannabinoid system in the gut. While CB2 receptor shows relevant role in mucosal immunity, being expressed prevalently on intestinal macrophages, CB1 receptor seems to be expressed in smooth muscle, submucosal myenteric plexus and normal human colon (Wright et al, 2005). The intricate regulation of this system seems to be contest- and cell-specific and may totally differ depending on patho-physiological conditions, but the exact regulation must still be clarified to optimize clinical use of specific cannabinoid compounds. Some authors reported that acute administration of Rimonabant (3 and 5.6 mg/kg dose), increases gastrointestinal motility, diarrhoea and nausea, in dose-dependent manner. However, Carai and collegues (2004) demonstrated that in mice, after initial induction of intestinal peristalsis, tolerance mechanisms occur (Izzo et al, 2010; Carai et al, 2004). Of course, since normal colon organoids contain all cell type of intestinal crypt and villus compartments (e.g. Lgr5+ niche stem cells, goblet cells, Paneth cells etc.) (Leushacke & Barker, 2014), with these results we cannot establish if Rimonabant influences differentiation or, generally, homeostasis of normal epithelium, in cell-specific manner. Thus, additional experiments would be needed to deepen this aspect.

Overall, emerging results from this work depicted a completely novel and unexplored mechanism for CB1 receptor inverse agonist, Rimonabant.

Described results allow us to candidate Rimonabant as a novel lead compound, able to control, *in vitro* and *in vivo,* Wnt/β-Catenin pathway with both direct inhibition of canonical signaling in β-Catenin mutant CRC cells and through p300 HAT activity inhibition. For the first time Rimonabant was reported to be an epigenetic modulator in CRC, able to eradicate colon CSCs population. Finally, our preliminary results on normal colon human organoids, seems to suggest Rimonabant selectivity toward cancer cells.

Ongoing experiments will help us to clarify and to dissect the mechanisms and the selective targets of the Rimonabant-mediated epigenetic effects. . Moreover, since obtained results in GTG7 cells seems to be promising, we will clarify the role of this compound in CSCs biology.

Acknowledgments.

References

Aguado T, Carracedo A, Julien B, Velasco G, Milman G, Mechoulam R, Alvarez L, Guzmán M, Galve-Roperh I. Cannabinoids induce glioma stem-like differentiation and inhibit gliomagenesis. *The Journal Of Biological Chemistry* Vol. 282, No. 9, pp. 6854–6862, March 2, 2007

Anastas JM and Moon RT. WNT signalling pathways as therapeutic targets in cancer. *Nature Reviews Cancer* 2013; 13: 11-26.

Bardelli A, Siena S. Molecular mechanisms of resistance to cetuximab and panitumumab in colorectal cancer. *J Clin Oncol* 2010; 28: 1254-61.

Bordonaro M, Lazarova DL. Determination of the Role of CBP- and p300-Mediated Wnt Signaling on Colonic Cells. *JMIR Res Protoc*. 2016 May 13;5(2):e66. doi:10.2196/resprot.5495.

Carai MA, Colombo G, Gessa GL. Rapid tolerance to the intestinal prokinetic effect of cannabinoid CB1 receptor antagonist, SR 141716 (Rimonabant). *Eur J Pharmacol*. 2004 Jun 28;494(2-3):221-4.

Castellone MD, Teramoto H, Williams BO, Druey KM, Gutkind JS. Prostaglandin E2 promotes colon cancer cell growth through a Gs-axin-beta-catenin signaling axis. *Science* 2005; 310: 1504-10.

Chou TC, Talalay P. Quantitative analysis of dose-effect relationships: the combined effects of multiple drugs or enzyme inhibitors. *Adv Enzyme Regul*. 1984;22:27-55.

Chou TC. Drug Combination Studies and Their Synergy Quantification Using the Chou-Talalay Method. *Cancer Res*, 2010 (70) (2) 440-446; DOI: 10.1158/0008-5472.CAN-09-1947

Ciaglia E, Torelli G, Pisanti S, Picardi P, D'Alessandro A, Laezza C, Malfitano AM, Fiore D, Pagano Zottola AC, Proto MC, Catapano G, Gazzerro P, Bifulco M. Cannabinoid receptor CB1 regulates STAT3 activity and its expression dictates the responsiveness to SR141716 treatment in human glioma patients' cells. *Oncotarget*. 2015 Jun 20;6(17):15464-81.

Cianchi F, Papucci L, Schiavone N, Lulli M, Magnelli L, Vinci MC, Messerini L, Manera C, Ronconi E, Romagnani P, Donnini M, Perigli G, Trallori G, Tanganelli E, Capaccioli S, Masini E. Cannabinoid receptor activation induces apoptosis through tumor necrosis factor alpha-mediated ceramide de novo synthesis in colon cancer cells. *Clin Cancer Res*. 2008 Dec 1;14(23):7691-700.

Deitrick J, Pruitt WM. Wnt/β Catenin-Mediated Signaling Commonly Altered in Colorectal Cancer. *Prog Mol Biol Transl Sci*. 2016;144:49-68. doi: 10.1016/bs.pmbts.2016.09.010

DeMorrow S, Francis H, Gaudio E, Venter J, Franchitto A, Kopriva S Onori P, Mancinelli R, Frampton G, Coufal M, Mitchell B, Vaculin B, Alpini G. The endocannabinoid anandamide inhibits cholangiocarcinoma growth via activation of the noncanonical Wnt signaling pathway. *Am J Physiol Gastrointest Liver Physiol* 2008; 295: G1150-8.

Fearon ER. Molecular genetics of colorectal cancer. *Annu Rev Pathol*. 2011;6:479-507. doi: 10.1146/annurev-pathol-011110-130235. Review.

Gaddis M, Gerrard D, Frietze S, Farnham PJ. Altering cancer transcriptomes using epigenomic inhibitors. *Epigenetics Chromatin*. 2015 Feb 24;8:9. doi:10.1186/1756-8935-8-9.

Gazzerro P, Malfitano AM, Proto MC, Santoro A, Pisanti S, Caruso MG Notarnicola M, Messa C, Laezza C, Misso G, Caraglia M, Bifulco M. Synergistic inhibition of human colon cancer cell growth by the cannabinoid CB1 receptor antagonist rimonabant and oxaliplatin. *Oncol Rep* 2010; 23: 171-5.

Greenhough A, Patsos HA, Williams AC, Paraskeva C. The cannabinoid delta(9)-tetrahydrocannabinol inhibits RAS-MAPK and PI3K-AKT survival signalling and induces BAD-mediated apoptosis in colorectal cancer cells. *Int J Cancer*. 2007 Nov 15;121(10):2172-80.

Guinney J, Dienstmann R, Wang X, de Reyniès A, Schlicker A, Soneson C, Marisa L, Roepman P, Nyamundanda G, Angelino P, Bot BM, Morris JS, Simon IM, Gerster S, Fessler E, De Sousa E Melo F, Missiaglia E, Ramay H, Barras D, Homicsko K, Maru D, Manyam GC, Broom B, Boige V, Perez-Villamil B, Laderas T, Salazar R, Gray JW, Hanahan D, Tabernero J, Bernards R, Friend SH, Laurent-Puig P, Medema JP, Sadanandam A, Wessels L, Delorenzi M, Kopetz S, Vermeulen L, Tejpar S. The consensus molecular subtypes of colorectal cancer. *Nat Med*. 2015 Nov;21(11):1350-6. doi: 10.1038/nm.3967.

Gustafsson SB, Lindgren T, Jonsson M, Jacobsson SO. Cannabinoid receptor-independent cytotoxic effects of cannabinoids in human colorectal carcinoma cells: synergism with 5-fluorouracil. *Cancer Chemother Pharmacol* 2009; 63(4): 691-701.

Herbst A, Jurinovic V, Krebs S, Thieme SE, Blum H, Göke B, Kolligs FT. Comprehensive analysis of β-catenin target genes in colorectal carcinoma cell lines with deregulated WNT/β-catenin signaling. *BMC Genomics* 2014; 15: 74.

Hertzman Johansson C, Egyhazi Brage S. BRAF inhibitors in cancer therapy. *Pharmacol Ther* 2014; 142: 176-82.

Hsu HC, Liu YS, Tseng KC, Hsu CL, Liang Y, Yang TS, Chen JS, Tang RP, Chen SJ, Chen HC. Overexpression of Lgr5 correlates with resistance to 5-FU-based chemotherapy in colorectal cancer. *Int J Colorectal Dis*. 2013 Nov;28(11):1535-46. doi: 10.1007/s00384-013-1721-x.

Ishitani T, Kishida S, Hyodo-Miura J, Ueno N, Yasuda J, Waterman M, Shibuya H, Moon RT, Ninomiya-Tsuji J, Matsumoto K. The TAK1-NLK mitogen-activated protein kinase cascade functions in the Wnt-5a/Ca(2+) pathway to antagonize Wnt/beta-catenin signaling. *Mol Cell Biol* 2003; 23: 131-9.

Izzo AA, Aviello G, Petrosino S, Orlando P, Marsicano G, Lutz B, Borrelli F, Capasso R, Nigam S, Capasso F, Di Marzo V. Increased endocannabinoid levels reduce the development of precancerous lesions in the mouse colon. *J Mol Med* (Berl) 2008; 86: 89-98.

Izzo AA, Sharkey KA. Cannabinoids and the gut: new developments and emergingconcepts. *Pharmacol Ther*. 2010 Apr;126(1):21-38. doi:10.1016/j.pharmthera.2009.12.005. Review.

Jacobs KM, Bhave SR, Ferraro DJ, Jaboin JJ, Hallahan DE, Thotala D. GSK-3β: A Bifunctional Role in Cell Death Pathways. *Int J Cell Biol* 2012; 2012: 930710.

Jhawer M, Goel S, Wilson AJ, Montagna C, Ling YH, Byun DS, Nasser S, Arango D, Shin J, Klampfer L, Augenlicht LH, Perez-Soler R, Mariadason JM. PIK3CA mutation/PTEN expression status predicts response of colon cancer cells to the epidermal growth factor receptor inhibitor cetuximab. *Cancer Res* 2008; 68: 1953-61.

Johnson V, Volikos E, Halford SE, Eftekhar Sadat ET, Popat S, Talbot I, Truninger K, Martin J, Jass J, Houlston R, Atkin W, Tomlinson IP, Silver AR. Exon 3 beta-catenin mutations are specifically associated with colorectal carcinomas in hereditary non-polyposis colorectal cancer syndrome. *Gut*. 2005 Feb;54(2):264-7.

Kemper K, Grandela C, Medema JP. Molecular identification and targeting of colorectal cancer stem cells. *Oncotarget*. 2010 Oct;1(6):387-95. Review.

Kimelman D, Xu W. Beta-catenin destruction complex: insights and questions from a structural perspective. *Oncogene* 2006; 25: 7482–7491.

LaBonte MJ, Wilson PM, Fazzone W, Russell J, Louie SG, El-Khoueiry A Lenz HJ, Ladner RD. The dual EGFR/HER2 inhibitor lapatinib synergistically enhances the antitumor activity of the histone deacetylase

inhibitor panobinostat in colorectal cancer models. *Cancer Res* 2011; 71: 3635-48.

Laezza C, D'Alessandro A, Paladino S, Maria Malfitano A, Chiara Proto M, Gazzerro P, Pisanti S, Santoro A, Ciaglia E, Bifulco M. Anandamide inhibits the Wnt/β-catenin signalling pathway in human breast cancer MDA MB 231 cells. *Eur J Cancer* 2012; 48: 3112-22

Lauro G, Masullo M, Piacente S, Riccio R, Bifulco G. Inverse Virtual Screening allows the discovery of the biological activity of natural compounds. *Bioorg Med Chem.* 2012 Jun 1;20(11):3596-602. doi: 10.1016/j.bmc.2012.03.072.

Lauro G, Romano A, Riccio R, Bifulco G. Inverse virtual screening of antitumor targets: pilot study on a small database of natural bioactive compounds. *J Nat Prod.* 2011 Jun 24;74(6):1401-7. doi: 10.1021/np100935s.

Lee, H. J., Wang, N. X., Shi, D. L. & Zheng, J. J. Sulindac inhibits canonical Wnt signaling by blocking the PDZ domain of the protein Dishevelled. *Angew. Chem. Int. Ed. Engl.* 48, 6448–6452 (2009).

Lenz HJ, Kahn M. Safely targeting cancer stem cells via selective catenin coactivator antagonism. *Cancer Sci.* 2014 Sep;105(9):1087-92. doi:10.1111/cas.12471.

Leushacke M, Barker N. Ex vivo culture of the intestinal epithelium: strategies and applications. *Gut.* 2014 Aug;63(8):1345-54. doi: 10.1136/gutjnl-2014-307204. Review.

Liu J, Pan S, Hsieh MH, Ng N, Sun F, Wang T Kasibhatla S, Schuller AG, Li AG, Cheng D, Li J, Tompkins C, Pferdekamper A, Steffy A, Cheng J, Kowal C, Phung V, Guo G, Wang Y, Graham MP, Flynn S, Brenner JC, Li C, Villarroel MC, Schultz PG, Wu X, McNamara P, Sellers WR, Petruzzelli L, Boral AL, Seidel HM, McLaughlin ME, Che J, Carey TE, Vanasse G, Harris JL. Targeting Wnt-driven cancer through the inhibition of Porcupine by LGK974. *Proc Natl Acad Sci* U S A 2013; 110: 20224-9.

Maida V, Daeninck PJ. A user's guide to cannabinoid therapies in oncology. *Curr Oncol.* 2016 Dec;23(6):398-406. doi: 10.3747/co.23.3487. Review.

Mikels AJ, Nusse R. Purified Wnt5a protein activates or inhibits beta-catenin-TCF signaling depending on receptor context. *PLoS Biol* 2006; 4: e115.

Morin PJ, Sparks AB, Korinek V, et al. Activation of beta-catenin-Tcf signaling in colon cancer by mutations in beta-catenin or APC. *Science.* 1997;275(5307):1787–1790.

Mosimann C, Hausmann G, Basler K. Beta-catenin hits chromatin: regulation of Wnt target gene activation. *Nat Rev Mol Cell Biol*. 2009 Apr;10 (4):276-86. doi:10.1038/nrm2654. Review.

Nabissi M, Morelli MB, Amantini C, Liberati S, Santoni M, Ricci-Vitiani L, Pallini R, Santoni G. Cannabidiol stimulates Aml-1a-dependent glial differentiation and inhibits glioma stem-like cells proliferation by inducing autophagy in a TRPV2-dependent manner. *Int J Cancer*. 2015 Oct 15;137(8):1855-69. doi: 10.1002/ijc.29573.

Nomachi A, Nishita M, Inaba D, Enomoto M, Hamasaki M, Minami Y. Receptor tyrosine kinase Ror2 mediates Wnt5a-induced polarized cell migration by activating c-Jun N-terminal kinase via actin-binding protein filamin A. *J Biol Chem* 2008; 283: 27973-81.

Nuñez F, Bravo S, Cruzat F, Montecino M, De Ferrari GV. Wnt/β-catenin signaling enhances cyclooxygenase-2 (COX2) transcriptional activity in gastric cancer cells. *PLoS One* 2011; 6: e18562.

O'Boyle NM, Banck M, James CA, Morley C, Vandermeersch T, Hutchison GR. Open Babel: An open chemical toolbox. *J Cheminform*. 2011 Oct 7;3:33. doi:10.1186/1758-2946-3-33.

O'Brien CA, Pollett A, Gallinger S, Dick JE. A human colon cancer cell capable of initiating tumour growth in immunodeficient mice. *Nature*. 2007 Jan 4;445(7123):106-10.

Ohta Y, Sato T. Intestinal tumor in a dish. *Front Med* (Lausanne). 2014 May 30;1:14. doi: 10.3389/fmed.2014.00014. Review.

Oishi I, Suzuki H, Onishi N, Takada R, Kani S, Ohkawara B Koshida I, Suzuki K, Yamada G, Schwabe GC, Mundlos S, Shibuya H, Takada S, Minami Y. The receptor tyrosine kinase Ror2 is involved in non-canonical Wnt5a/JNK signalling pathway. *Genes Cells* 2003; 8: 645-54.

Paldino E, Tesori V, Casalbore P, Gasbarrini A, Puglisi MA. Tumor initiating cells and chemoresistance: which is the best strategy to target colon cancer stem cells? *Biomed Res Int*. 2014;2014:859871. doi: 10.1155/2014/859871. Review.

Patsos HA, Hicks DJ, Dobson RR, Greenhough A, Woodman N, Lane JD Williams AC, Paraskeva C. The endogenous cannabinoid, anandamide, induces cell death in colorectal carcinoma cells: a possible role for cyclooxygenase 2. *Gut* 2005; 54: 1741-50.

Prasetyanti PR, Zimberlin C, De Sousa E Melo F, Medema JP. Isolation and propagation of colon cancer stem cells. *Methods Mol Biol.* 2013;1035:247-59. doi: 10.1007/978-1-62703-508-8_21.

Proto MC, Gazzerro P, Di Croce L, Santoro A, Malfitano AM, Pisanti S, Laezza C, Bifulco M. Interaction of endocannabinoid system and steroid hormones in the control of colon cancer cell growth. *J Cell Physiol* 2012; 227: 250-8

Punt CJ, Koopman M, Vermeulen L. From tumour heterogeneity to advances in precision treatment of colorectal cancer. *Nat Rev Clin Oncol*. 2016 Dec 6. doi:10.1038/nrclinonc.2016.171.

Santoro A, Pisanti S, Grimaldi C, Izzo AA, Borrelli F, Proto MC, Malfitano AM, Gazzerro P, Laezza C, Bifulco M. Rimonabant inhibits human colon cancer cell growth and reduces the formation of precancerous lesions in the mouse colon. *Int J Cancer* 2009; 125: 996-1003.

Sato T, Stange DE, Ferrante M, Vries RG, Van Es JH, Van den Brink S, Van Houdt WJ, Pronk A, Van Gorp J, Siersema PD, Clevers H. Long-term expansion of epithelial organoids from human colon, adenoma, adenocarcinoma, and Barrett's epithelium. *Gastroenterology*. 2011 Nov;141(5):1762-72. doi: 10.1053/j.gastro.2011.07.050.

Sharma, M., Hudson, J., Adomat, H., Guns, E. & Cox, M. *In Vitro* Anticancer Activity of Plant-Derived Cannabidiol on Prostate Cancer Cell Lines. *Pharmacology & Pharmacy*, 2014. 5, 806-820.

Stamos JL, Weis WI. The β-catenin destruction complex. *Cold Spring Harb Perspect Biol* 2013; 5: a007898.

Takebe N, Miele L, Harris PJ, Jeong W, Bando H, Kahn M, Yang SX, Ivy SP. Targeting Notch, Hedgehog, and Wnt pathways in cancer stem cells: clinical update. *Nat Rev Clin Oncol*. 2015 Aug;12(8):445-64. doi: 10.1038/nrclinonc.2015.61. Review.

Todaro M, Francipane MG, Medema JP, Stassi G. Colon cancer stem cells: promise of targeted therapy. *Gastroenterology*. 2010 Jun;138(6):2151-62. doi:10.1053/j.gastro.2009.12.063.

Trott O, Olson AJ. AutoDock Vina: improving the speed and accuracy of docking with a new scoring function, efficient optimization, and multithreading. *J Comput Chem*. 2010 Jan 30;31(2):455-61. doi: 10.1002/jcc.21334.

Tuynman JB, Vermeulen L, Boon EM, Kemper K, Zwinderman AH, Peppelenbosch MP, Richel DJ. Cyclooxygenase-2 inhibition inhibits c-Met kinase activity and Wnt activity in colon cancer. *Cancer Res*. 2008 Feb 15;68(4):1213-20. doi:10.1158/0008-5472.CAN-07-5172.

Velasco G, Sánchez C, Guzmán M. Anticancer mechanisms of cannabinoids. *Curr Oncol*. 2016 Mar;23(2):S23-32. doi: 10.3747/co.23.3080

Vermeulen L, De Sousa E Melo F, van der Heijden M, Cameron K, de Jong JH, Borovski T, Tuynman JB, Todaro M, Merz C, Rodermond H, Sprick MR, Kemper K, Richel DJ, Stassi G, Medema JP. Wnt activity defines colon cancer stem cells and is regulated by the microenvironment. *Nat Cell Biol*. 2010 May;12(5):468-76. doi: 10.1038/ncb2048.

Vlad A, Röhrs S, Klein-Hitpass L, Müller O. The first five years of the Wnt targetome. *Cell Signal* 2008; 20: 795-802.

Wang D, Wang H, Ning W, Backlund MG, Dey SK, DuBois RN. Loss of cannabinoid receptor 1 accelerates intestinal tumor growth. *Cancer Res.* 2008; 68(15):6468-76.

Wang L, Liu X, Gusev E, Wang C, Fagotto F. Regulation of the phosphorylation and nuclear import and export of β-catenin by APC and its cancer-related truncated form. *J Cell Sci*. 2014 Apr 15;127(Pt 8):1647-59. doi:10.1242/jcs.131045.

Wright K, Rooney N, Feeney M, Tate J, Robertson D, Welham M, Ward S. Differential expression of cannabinoid receptors in the human colon: cannabinoids promote epithelial wound healing. *Gastroenterology*. 2005 Aug;129(2):437-53.

Yang J, Zhang W, Evans PM, Chen X, He X, Liu C. Adenomatous polyposis coli (APC) differentially regulates beta-catenin phosphorylation and ubiquitination in colon cancer cells. *J Biol Chem* 2006; 281: 17751-7.

Ying J, Li H, Yu J, Ng KM, Poon FF, Wong SC, Chan AT, Sung JJ, Tao Q. WNT5A exhibits tumor-suppressive activity through antagonizing the Wnt/beta-catenin signaling, and is frequently methylated in colorectal cancer. *Clin Cancer Res* 2008; 14: 55-61.

Zeuner A, Todaro M, Stassi G, De Maria R. Colorectal cancer stem cells: from the crypt to the clinic. *Cell Stem Cell*. 2014 Dec 4;15(6):692-705. doi:10.1016/j.stem.2014.11.012. Review.

Zhang HH, Walker F, Kiflemariam S, Whitehead RH, Williams D, Phillips WA et al. Selective inhibition of proliferation in colorectal carcinoma cell lines expressing mutant APC or activated B-Raf. *Int J Cancer* 2009; 125: 297-307.

Zhao J. Cancer stem cells and chemoresistance: The smartest survives the raid. *Pharmacol Ther*. 2016 Apr; 160:145-58. doi:10.1016/j.pharmthera. 2016.02.008. Review.